PARITY MEASUREMENTS OBTAINED FROM THE $^{48}Ca(\vec{d},\alpha)^{46}K$ REACTION AT 4°

By

STEVEN ANGELO, B.SC.

A Thesis

Submitted to the School of Graduate Studies

in Partial Fulfilment of the Requirements

for the Degree

Master of Science

McMaster University

November 1979

PARITY MEASUREMENTS OBTAINED FROM THE $^{48}Ca(\vec{d},\alpha)^{46}K$ REACTION

MASTER OF SCIENCE (1979)
(Physics)

McMASTER UNIVERSITY
Hamilton, Ontario

TITLE: Parity Measurements Obtained from the $^{48}Ca(\vec{d},\alpha)^{46}K$ Reaction at 4°

AUTHOR: Steve Angelo, B.Sc. (McMaster University)

SUPERVISOR: Professor John A. Kuehner

NUMBER OF PAGES: xii, 63

Abstract

A polarized deuteron beam was used to initiate a (d,α) reaction on an even-even target with the detection of the reaction products near 0°. A model independent technique is utilized which allows the parity of a nuclear state (natural or unnatural) to be determined from a measurement of the tensor analyzing power T_{20}. In addition, it is possible to identify 0^- levels uniquely.

This reaction was performed on a doubly-magic ^{48}Ca target. The resulting isotope ^{46}K may therefore be treated as a proton hole and a neutron hole in a ^{48}Ca core. As a result of this simple shell-model picture, several investigations into the spins and parities of the low-lying states of ^{46}K have been conducted. However, some of these model dependent assignments have yielded contradictory results - hence the need for this study.

The $^{48}Ca(\vec{d},\alpha)^{46}K$ reaction was carried out at 4° with bombarding energies of 7.5, 8.0, 8.5, and 9.0 MeV. For a given beam energy, spectra obtained with the incident deuterons preferentially polarized in the m=0 substate were compared with spectra obtained with polarized deuterons in the m=1 substate. The following parities were deduced from the levels in ^{46}K: ground state, 0.69, 1.74, 1.94 MeV levels

(unnatural parity)

0.59 and 0.89 MeV levels (natural parity).

In addition, a tentative natural parity assignment was made to the 1.37 MeV state. The resulting spin-parity combinations are found to be consistent with the most recent set of measurements by Daehnick et.al.[2].

Pandya calculations were made in which the order and separation of the lowest levels of ^{40}K were obtained from the ^{46}K levels. As a result of configuration mixing, the calculations bear little resemblance to the experimental ^{40}K spectrum. A discussion of configuration mixing effects is also provided.

ACKNOWLEDGEMENTS

This thesis would not be complete without an acknowledgement* of the various people who have somehow influenced my postgraduate work. I would even like to thank some of them, starting with my supervisory committee:

Dr. John Kuehner, the best supervisor I've ever had, for his advice, encouragement, and patience. But, then, good doctors always have plenty of patience.

Aadu "hopefully" Pitt for his help during the experiments and for discussions pertaining to them.

John Cameron for his enthusiasm, optimism, and uncanny ability of keeping a straight face during my defense.

As well, I am much obliged to:

Arif Khan for showing me the ropes and for his assistance during the early runs,

M.A.M. Shahabuddin for some stimulating discussions,

John McKay for taming the polarized ion source,

Maria Krystalski for her superb work on my drawings and for providing a bit of cheesecake,

Helen Kennelly for her flawless typinj (sorry) and for deciphering the sections scrawled in crayon.

The staff and students at the tandem lab for their kindness and support which I shall find very difficult to repay.

And finally, a tip of the hat to the hermit Paul E. Nomial for agreeing to direct the movie version of this thesis.

* regulation 43, subsection 2

Without going out of his door,
He knows everything in the world.
Without looking out of his window
He knows the way to heaven.
The further we go,
The less we learn.

- Roshi
(translated by R.H. Bluth)

I read the news today oh boy
Four thousand holes in Blackburn, Lancashire
And though the holes were rather small
They had to count them all.
Now they know how many holes it takes to fill the
Albert Hall

- John Lennon and Paul McCartney
from "A Day In The Life" (1967)

He looks so truthful, is this how he feels
Trying to peel the moon and expose it

- Bob Dylan
from "Can You Please Crawl Out Your Window?" (1965)

TO The Authorities

Who Drink Their Coffee

With A Raised Pinky

Table of Contents

Chapter		page no.
	Descriptive Note	ii
	Abstract	iii
	Acknowledgements	v
	Table of Contents	viii
	List of Figures	x
	List of Tables	xii
I	Introduction	1
II	Theory	4
	II.1 Preamble	(4)
	II.2 The direct (d,α) reaction	(4)
	II.3 The $(\vec{d},\alpha)$ reaction at 0°	(6)
	II.4 Some practical considerations	(13)
III	Details of the Experiment	17
	III.1 Polarized ion source	(17)
	III.2 Apparatus and set-up	(18)
	III.3 More practical considerations	(22)
IV	Experimental Results	28
	IV.1 Analysis of data	(28)
	IV.2 Parity assignments and comparison with published results	(38)
V	Calculation and Discussion	46
	V.1 Pandya calculations	(46)
	V.2 $d_{3/2}$-$s_{1/2}$ spacing and configuration mixing effects	(49)

Chapter		page no.
	V.3 Consequences of mixing	(54)
VI	Concluding Remarks (abstract revisited)	57
	References	60
	Miscellaneous References	63
	Nuclear energy level references	63

List of Figures

Figure		page no.
III-1	The target vacuum lock system	20
III-2	Block diagram of the electronics	23
III-3	The energy loss spectrum from the $^{48}Ca(\vec{d},\alpha)^{46}K$ reaction at 4°	24
III-4	Spectra from the $^{16}O(\vec{d},\alpha)^{14}N$ reaction with E_d = 7.5 MeV and θ_{lab} = 4°	27
IV-1	Spectra from the $^{48}Ca(\vec{d},\alpha)^{46}K$ reaction with E_d = 7.5 MeV and θ_{lab} = 4°	29
IV-2	Spectra from the $^{48}Ca(\vec{d},\alpha)^{46}K$ reaction with E_d = 8.0 MeV and θ_{lab} = 4°	30
IV-3	Spectra from the $^{48}Ca(\vec{d},\alpha)^{46}K$ reaction with E_d = 8.5 MeV and θ_{lab} = 4°	31
IV-4	Spectra from the $^{48}Ca(\vec{d},\alpha)^{46}K$ reaction with E_d = 9.0 MeV and θ_{lab} = 4°	32
IV-5	Comparison of ^{38}K spectrum with ^{46}K spectrum for 7.5 MeV deuterons in the m=0 substate	35
IV-6	Comparison of ^{38}K spectrum with ^{46}K spectrum for 7.5 MeV deuterons in the m=1 substate	36
IV-7	The tensor analyzing powers for levels from the $^{48}Ca(\vec{d},\alpha)^{46}K$ reaction	39

Figure		page no.
V-1	The energy of the $s_{1/2}$ hole in ${}^{A}_{19}K$ vs. the mass number A	50
V-2a)	The energy level diagrams for ^{46}K, ^{40}K, and ^{38}Cl	53
V-2b)	A simplified representation of the lowest configurations for ^{46}K	53

List of Tables

Table		page no.
IV-1	^{46}K adopted levels and $\langle T_{20} \rangle$ values	41
V-1	Calculated energy levels of ^{38}Cl from ^{40}K using Pandya's theorem	48
V-2	Calculated energy levels of ^{40}K from ^{46}K using Pandya's theorem	48

CHAPTER I

INTRODUCTION

From the viewpoint of the shell model, the spectrum of ${}^{46}_{19}K_{27}$ should be an intriguing object of study, for in the most elementary analysis ${}^{46}K$ is only one proton hole and one neutron hole removed from the doubly magic nucleus ${}^{48}_{20}Ca_{28}$. The utilization of neutron-rich ${}^{48}Ca$ in a target enables the examination of reaction products with a conspicuous excess of neutrons. The determination of the spin-parity combinations of states in ${}^{46}K$ should yield important information on the structure of this nucleus.

The ${}^{46}K$ nucleus is a difficult one to obtain experimentally. It can only be procured from two nucleon transfer due to the lack of appropriate targets. Such reactions can reach states which typically can be described by a pair of nucleon holes excited with respect to the ground state; these two nucleon states cannot appear, in the lowest order, in inelastic or single nucleon transfer reactions. Hence, the earlier investigations of the spins and parities of ${}^{46}K$ levels consisted primarily of angular distribution measurements with (d,α) and (p,^{3}He) reactions. The ${}^{48}Ca(p,{}^{3}He){}^{46}K$ reaction was usually carried out in conjunction with ${}^{48}Ca(p,t){}^{46}Ca$ reactions leading to the comparison of $T = 4$ analog states.

Recently, $(d,\alpha\gamma)$ fast coincidence experiments[1,2] were performed to deduce ^{46}K level energies and spin limits. The resulting experimental evidence concerning the lowest lying levels of ^{46}K is, in some cases, contradictory mainly because the method of analysis depends upon the reaction mechanism.

In this work, ^{46}K levels up to approximately 2 MeV in excitation were investigated with a $(\vec{d},\alpha)$ experiment using beam energies ranging from 7.5 to 9.0 MeV. The use of polarized deuterons allows a model-independent way of assigning the parity of a nuclear state, spin J, as either natural $\pi = (-)^J$ or unnatural $\pi = (-)^{J+1}$. In addition, this model permits the determination of both spin and parity for the unique case of $J^\pi = 0^-$ levels. In certain situations, the spin J of a nuclear state can be found if previous results have somehow limited the choices of parity and spin.

For this method to work, it is essential that the following requirements[3] be met: a) An $m = 0$ polarized beam must be incident upon an even-even target nucleus and b) any $J^\pi = 0^+$ outgoing particles from this reaction should be detected at 0° or 180° to the direction of the beam.

Using information in the form of single hole energies, it can be assumed that the lowest two-hole states in ^{46}K have negative parity and the prominent configurations are $\pi d^{-1}_{3/2}\nu f^{-1}_{7/2}$ and $\pi s^{-1}_{1/2}\nu f^{-1}_{7/2}$. The expected levels, in the immediate vicinity of (and including) the ground state would consist of a $J^{\pi} = 2^{-}$ and 5^{-} state along with a pair of $J^{\pi} = 3^{-}$ and 4^{-} states. Data collected since the initial detection of this isotope by Marinov and Erskine[4] has indicated that this simple picture is inadequate. This will be discussed in greater length in chapter V.

CHAPTER II

THEORY

II.1 Preamble

For the particular case of the reaction carried out in this experiment, it is not clear, in retrospect, whether this reaction proceeded as a direct transfer of nucleons or through the formation of a compound nucleus. It seems quite likely that, for the beam energies used, neither reaction mechanism completely dominated the other; in fact, they may have even been in direct competition with each other. One should bear this in mind when one of these mechanisms is brought up during the following discussion in order to emphasize certain features.

II.2 The direct (d,α) reaction

As might be expected, two nucleon transfer reactions are not as well understood as the corresponding situation for a single nucleon. Only the salient features for direct reactions will be mentioned here. A very complete discussion of the theory of nucleon pair transfer reactions can be found in Glendenning[5,6].

An examination of spectra from a (d,α) reaction would show that it is quite selective in the levels that are excited. Statistical factors alone cannot account for the diversification in the intensities of these excited states. One must also consider the intrinsic structure of the excited levels themselves. For example, states that can be accurately depicted by configurations consisting of two holes in the unexcited target nucleus tend to be highly favoured.

The stripping amplitude, for two nucleon transfer reactions, can be factorized into two parts: a G factor containing nuclear structure information and a kinematic B factor containing the radial wavefunction $u_{NL}(\vec{R})$ for the nucleon pair in centre of mass coordinates. The differential cross-section can be expressed as an incoherent sum over the spin S, orbital L, and total J angular momenta plus the isospin T of the two transferred nucleons (quantum numbers NLSJ) of:

$$\sum_M \left| \sum_N G_{NLSJT} \, B^M_{NL} \right|^2 .$$

In contrast, the cross-section itself for single nucleon transfer reactions can be separated into a kinematic factor and a nuclear structure factor.

Different selection rules exist for different types of two nucleon transfer reactions. The resulting constraints for the case of a (d,α) reaction are simply:

(i) $$\vec{J} = \vec{J}_f - \vec{J}_i = \vec{j}_n + \vec{j}_p = \vec{L} + \vec{S}$$

where $\vec{L} = \vec{\ell}_n + \vec{\ell}_p$

(ii) $$\vec{T} = \vec{T}_f - \vec{T}_i = 0 \, .$$

If slight admixtures arising from non-central forces are neglected, the space wavefunction corresponds to relative s-state motion among the nucleons. Thus, the transferred neutron and proton can be assumed to have zero relative angular momentum. Consequently, this leads to the following rules:

(iii) $$\pi_i \pi_f = (-1)^L = (-1)^{\ell_n + \ell_p}$$

(iv) $$S = 1 \, .$$

For the special case of two nucleons transferred to or from the same spin-orbit state (identical $n\ell j$ quantum numbers) another selection rule can be derived:

$(j^2)_{J=\text{even}}$ pickup is strictly prohibited.

II.3 The $(\vec{d},\alpha)$ reaction at 0°

By preferentially aligning the deuterons in certain spatial orientations, one will be able to extract even more information from such a reaction. Much of the pioneering $(\vec{d},\alpha)$ work at the McMaster tandem lab was performed by Petty, Kuehner, et.al[7,8,9]. The development presented in the remainder of this chapter will follow closely the detailed account found in Petty[3].

The use of a polarized beam allows the measured cross-section to be expanded in terms of spherical tensor moments t_{kq}:

$$\frac{d\sigma}{d\Omega} = N \sum_{kq} T^{*}_{kq}\, t^{in}_{kq} \qquad (1).$$

where T_{kq} are the analyzing powers and N, the normalization constant, is just the unpolarized (u/p) cross-section.

Considerations of parity conservation, symmetry, and transformation properties ot T_{kq} lead to the following expression for spin 1 incident particles (such as deuterons):

$$\frac{d\sigma}{d\Omega} = \left(\frac{d\sigma}{d\Omega}\right)_{u/p} \{1 + 2i\, T_{11}\, \mathrm{Re}(it_{11}) + t_{20}\, T_{20}$$

$$+ 2\, T_{21}\, \mathrm{Re}(t_{21}) + 2\, T_{22}\, \mathrm{Re}(t_{22})\} \qquad (2)$$

The reaction amplitudes F^{i}_{m} can be expanded in terms of partial waves f^{i}_{m} and hence are separable into an angle dependent and angle independent part[10]. It is often very convenient to do so in the helicity frame. Here the z-axis is selected, in a centre of mass frame, for each particle along the direction of its momentum. The y-axis can then be chosen in a direction perpendicular to the plane of the reaction and is defined by $\vec{p}_{in} \times \vec{p}_{out}$ where $\vec{p}_{in}$ is the linear momentum of the deuteron and $\vec{p}_{out}$ is the linear momentum of the alpha particle.

$$F^{i}_{m} = \sum_{J} \frac{2J+1}{4\pi}\, f^{i}_{m}(J)\, d^{J}_{im}(\theta) \qquad (3)$$

Once parity conservation in the reaction is taken into account, the following relation can be written (for spin 1 particles):

$$F_{-m}^{-i} = \pi(-1)^{i+m+1+J}F_m^i \qquad (4)$$

where J is the spin of the residual nucleus and π is the product of the parities for the four particles present in the reaction. For a (d,α) reaction on an even-even target, this is equivalent to the parity of the final state in the residual nucleus.

The analyzing powers can be expanded in terms of the reaction amplitudes:

$$T_{kq} = \frac{1}{N} \sum_{imj} (\tau_{kq}^{s=1})_{ij} \; F_m^i \; F_m^{*j} \; . \qquad (5)$$

Here τ_{kq} are the spherical tensor operators and N is a normalization constant, usually chosen so that $T_{00} = 1$.

Most of the expressions given above can be further simplified if the alpha particles are detected at 0° (or 180°) to the beam direction. In equation (3), for example, the d function is non-zero only for i=m; this is simply a result of the conservation of angular momentum. Because $(\tau_{kq})_{mm} \propto \delta_{qo}$, all the tensor analyzing powers in (2) are zero, except for T_{20}. Accordingly, for this special geometry, the expression for the cross-section becomes:

$$\frac{d\sigma}{d\Omega} = \left(\frac{d\sigma}{d\Omega}\right)_{u/p} \{1 + t_{20}T_{20}\}. \qquad (6)$$

Equation (5) can also be modified to become:

$$T_{kq} = \frac{1}{N} \sum_{m} (\tau_{kq}^{s=1})_{mm} \left|F_m^m\right|^2 . \tag{7}$$

For s=1, the spherical tensor operators required for our purposes are:

$$\tau_{00} = 1 \tag{8a}$$

and

$$\tau_{20} = \frac{1}{\sqrt{2}} (3s_z^2 - 2) \tag{8b}$$

where s_z is the angular momentum operator. The normalization constant N can now be determined:

$$N = \sum_{m} (\tau_{00}^{s=1})_{mm} \left|F_m^m\right|^2$$

$$N = \left|F_{-1}^{-1}\right|^2 + \left|F_0^0\right|^2 + \left|F_1^1\right|^2 . \tag{9}$$

Consequently,

$$T_{20} = \frac{1}{N} \frac{\left|F_{-1}^{-1}\right|^2 - 2\left|F_0^0\right|^2 + \left|F_1^1\right|^2}{\sqrt{2}}$$

$$T_{20} = \frac{1}{\sqrt{2}} \frac{\left|F_{-1}^{-1}\right|^2 - 2\left|F_0^0\right|^2 + \left|F_1^1\right|^2}{\left|F_{-1}^{-1}\right|^2 + \left|F_0^0\right|^2 + \left|F_1^1\right|^2} \tag{10}$$

and the unpolarized cross-section is given by:

$$\left(\frac{d\sigma}{d\Omega}\right)_{u/p} = \frac{1}{3} \left\{\left|F_{-1}^{-1}\right|^2 + \left|F_0^0\right|^2 + \left|F_1^1\right|^2\right\}. \tag{11}$$

The parity conservation relation (4) for the scattering amplitudes may now be employed. For the case of a natural parity state $\pi = (-)^J$ the following results may be obtained

$$F_0^0 = -F_0^0 = 0$$

and

$$F_{-1}^{-1} = -F_1^1$$

so that equation (10) becomes

$$T_{20} = \frac{1}{\sqrt{2}} \text{ (for } \pi = (-)^J) . \tag{12}$$

The particular case of a spin zero will now be dealt with, in a similar manner. Here, the amplitudes F_1^1, F_{-1}^{-1} are strictly forbidden. A $J^\pi = 0^+$ state has $F_0^0 = 0$ and thus

$$\left(\frac{d\sigma}{d\Omega}\right)_{u/p} = 0 \qquad \text{(for } J^\pi = 0^+) . \tag{13}$$

For a $J^\pi = 0^-$ state, however, the relation (4) only furnishes the trivial result $F_0^0 = F_0^0$. This provides the result:

$$T_{20} = -\sqrt{2} \qquad \text{(for } J^\pi = 0^-) . \tag{14}$$

Note that thus far into this discussion, all the results have been model-independent. However, this does not hold for the situation concerning an unnatural parity state. The tensor analyzing power T_{20} can assume any value in between and including the limits represented by 0^- and natural parity states. This value depends solely upon the ratio F_0^0/F_1^1. As reaction amplitudes can only be calculated by assuming some mechanism for the reaction, it must be concluded that T_{20} for an unnatural parity state must, necessarily, be model dependent.

The tensor polarization t_{20} depends only upon two quantities: the magnetic substate of the beam and the degree to which the beam is totally polarized. The latter quantity is indicated by the fractional beam polarization p which is simply the fraction of the total beam current that is polarized. The values of t_{20} can be given as:

$$t_{20} = \frac{p}{\sqrt{2}} \qquad \text{for } m = \pm 1 \tag{15a}$$

$$t_{20} = -\sqrt{2}\, p \quad \text{for } m = 0 \; . \tag{15b}$$

The substitution of these results in equation (6) for a natural parity state (12) yields the relations given below for the measured cross-sections:

$$\left(\frac{d\sigma}{d\Omega}\right)_{m=0} = \left(\frac{d\sigma}{d\Omega}\right)_{u/p} (1-p) \tag{16a}$$

$$\left(\frac{d\sigma}{d\Omega}\right)_{m=1} = \left(\frac{d\sigma}{d\Omega}\right)_{u/p} \left(1 + \frac{p}{2}\right) . \tag{16b}$$

This implies that for a 100% polarized beam in the m=0 substate, there will be no measurable cross-section at 0° for a natural parity state. However, in practice, this is not so; there are always some unpolarized components present in the beam and one cannot measure at exactly 0° because of finite detector effects.

For the purposes of this experiment, the deuteron beam used was polarized in the m=0 and m=1 substates (relative to the direction of the incident beam) alternately. The cross-sections obtained in the m=0 substate were then compared with those measured in the m=1 substate. An expression relating this comparison to the tensor analyzing power will now be derived. Let R represent the ratio of the normalized peak intensities obtained in the m=0 and m=1 substates:

$$R = \frac{Y(m=0)}{Y(m=1)} = \frac{\left(\frac{d\sigma}{d\Omega}\right)_{m=0}}{\left(\frac{d\sigma}{d\Omega}\right)_{m=1}} \quad . \tag{17}$$

The substitution of equations (15a), (15b), and (6) into the above relation gives:

$$R = \frac{1 - \sqrt{2}\, p\, T_{20}}{1 + \frac{p}{\sqrt{2}} T_{20}}$$

assuming, of course, that the polarization does not change appreciably from one substate to the other.

One may now solve for T_{20} obtaining the useful result:

$$T_{20} = \frac{1}{\sqrt{2}\,p}\,\frac{1 - R}{1 + \frac{R}{2}} \,. \tag{19}$$

Alternatively, R may be defined as the ratio between the cross-sections obtained in the m=0 substate and from using an unpolarized beam:

$$R = \frac{\left(\frac{d\sigma}{d\Omega}\right)_{m=0}}{\left(\frac{d\sigma}{d\Omega}\right)_{u/p}} \,. \tag{20}$$

It is then a very simple matter to obtain

$$T_{20} = \frac{1}{\sqrt{2}\,p}\,(1-R)\,. \tag{21}$$

<u>II.4 Some practical considerations</u>

As previously discussed, it is possible for the tensor analyzing power for unnatural parity states to masquerade as 0^- or natural parity levels, at certain energies. It remains to be investigated for how many different energies T_{20} must be measured at the limits before it can reasonably be concluded to be a 0^- or natural parity state.

The scattering amplitude F may be written as the sum of an average part F_{av} and a fluctuating part, F_{fl}, if one assumes a statistical model[11] for the reaction. At the appropriate excitation energies that correspond to the continuum region, the width of the energy levels is greater than the level spacing. The numerous states overlapping with a given level contribute coherently, but randomly, to the scattering amplitude, thereby producing the fluctuating part[12]. The square of the scattering amplitudes can be averaged over energy to produce:

$$\langle F^2 \rangle = |F_{av}|^2 + \langle F_{fl}\ F_{fl}^* \rangle \ . \tag{22}$$

This can be interpreted to represent a direct reaction contribution from the first term and a compound nucleus contribution from the fluctuating second term. The tensor analyzing power will be affected the most by a pure compound nuclear reaction. This can be achieved by setting F_{av} to zero. If there are any direct contributions to the reaction performed in this experiment, they will only serve to dampen the extent of the fluctuations in T_{20}.

The previous condition implies a χ^2 probability distribution depending upon $|F|^2$ and its mean over energy $\langle |F|^2 \rangle$. For the case of measurements using several beam energies or, alternatively, a thick target the distribution becomes:

$$P(y) \propto \left(\frac{y}{\langle y \rangle}\right)^{N-1} \exp\left(-\frac{y}{\langle y \rangle}\right) \tag{23}$$

where y is $|F|^2$ and N depends upon the energy loss of the beam due to target thickness, in units of coherence width. In practice, resolution effects would hamper the use of sufficiently thick targets in an experiment. Instead, one could take an energy average for N different beam energies with a minimum separation of a coherence width.

Equations (10) and (23) may then be combined to obtain a probability distribution of T_{20} in terms of T_{20}, N, $<|F_1^1|^2>$ and $<|F_0^0|^2>$. Boerma et.al.[13] use a statistical weight argument to relate the average values of the scattering amplitudes in compound nuclear representation by

$$<|F_0^0|^2> = 2<|F_1^1|^2>. \qquad (24)$$

It should be mentioned that this analysis takes into account the various ℓ values contributing to the reaction. The last two equations (23,24) may be merged to give the following results. If a single beam energy is used on a thin target, the probability distribution is absolutely uniform between the two limits. For a greater number of beam energies, the distribution peaks at, and is symmetric about, $T_{20} = \frac{-1}{2\sqrt{2}}$, the midpoint between the limits. Of course, this is only an approximation based on (24) and for low beam energies will tend to approach $T_{20} = 0$[3,8]. The more energies N used during an experiment, the sharper the distribution will be about the maximum. Thus, it will be more and more unlikely for T_{20} for an unnatural parity state to be at one of the limits as N is increased. Petty[3,8] has estimated a 0.1% probability of obtaining an average T_{20} value closer than 0.1

to either limit for N=3. Three or more beam energies should certainly be adequate to assign a natural parity or $J^{\pi} = 0^{-}$ to a state.

One problem remains to be solved: that of detecting alpha particles at zero degrees. The finite size of the detector itself coupled with the fact that the deuterons in the beam cannot possibly be stopped from entering the counter without also obstructing the alpha particles renders this condition impractical. As a result, measurements must be made at small, but non-zero, angles to the beam.

Under these circumstances, the expression for the tensor analyzing power for natural parity or 0^{-} states becomes extremely involved and model dependent. The average attenuation of T_{20} can be assessed by employing a statistical model calculation using Coulomb penetrabilities. The final results are functions only of the target nucleus radius, beam energy, and final state excitation energy. An estimate of the magnitude of this attenuation will be offered in the next chapter.

A preliminary investigation into the effect of assuming a direct transfer reaction instead of the compound nuclear reaction considered above seems to indicate that there will be no significant alteration of the T_{20} attenuation with angle. It also appears that although under the proper circumstances a direct reaction may yield a T_{20} value, for an unnatural parity state, close to one of the limits, there is an extremely remote possibility of this occurring[14].

CHAPTER III

DETAILS OF THE EXPERIMENT

III.1 Polarized ion source

The polarized deuteron beam was supplied by the McMaster Lamb-shift polarized ion source. A detailed description of this source is given by McKay[15]. A brief account of its operation follows.

A beam of unpolarized positive deuterium ion is produced by a duoplasmatron source and is extracted with approximately 7 keV energy. The deuterons are then slowed down to about 1 keV so that the charge exchange processes that follow are optimized. A caesium vapour canal is entered next where neutral atoms in their metastable 2s state are formed with approximately 30% efficiency along with neutral ground state atoms and charged ions. In addition, the caesium vapour allows some space charge cancellation thus reducing the spreading out of the charged beam. The ensuing spin filter region utilizes the appropriate electric and magnetic fields to selectively quench all but the desired m state to the ground state and to deflect the undesired charged constituents out of the beam.

Subsequently, the beam passes through an argon charge exchange canal where the 2s deuterium atoms form negative ions with a probability that is a couple of orders of magnitude higher than for the unpolarized ground state atoms (for a kinetic energy of 1 keV). The negative-ion beam is then accelerated and focussed through a three gap lens system and injected into the regular FN Tandem Van de Graaff accelerator system with an energy of nearly 70 keV. A Wien filter consisting of crossed electric and magnetic fields, mutually perpendicular to the beam, allows the precession of the polarization axis through an appropriate angle such that the quantization axis is aligned along the beam direction when the beam finally enters the target chamber.

III.2 Apparatus and set-up

Two quartz viewers, situated before the target chamber were employed to allow observation of the beam in order to facilitate the setting of the steering and focussing elements. A 1 mm diameter aperture, located in the target ladder itself, enabled a fine tuning in the focussing and steering to be undertaken. An Enge split-pole magnetic spectrograph[16,17] was used to momentum analyze and focus the alpha particles produced by the reaction. These were then detected on the focal plane with a position-sensitive gas proportional counter[18,19]. The measurements were taken at 4° to the beam direction in the lab system with beam energies of 7.5, 8.0, 8.5 and 9.0 MeV.

A special Faraday cup system was utilized for this experiment. It consisted of two concentric arcs of tantalum isolated from each other by insulating spacers. The inner metallic curve had a longitudinal slit cut into it allowing the beam to pass through it. A potential of minus 300 volts was applied to this section to suppress secondary electron current produced by the interaction of the beam. The tantalum arc furthest from the target acted as a Faraday cup. This entire assembly was mounted in the target chamber with an insulating teflon insert fitting snugly into the valve opening between the target chamber and the spectrograph. A rectangular aperture (7mm × 8 mm) in the Faraday cup permitted the alphas to enter the magnet chamber. This whole arrangement was free to slide on a plastic pillbox support so that measurements could be taken out as far as 30° to the beam path if required.

The targets for this experiment were evaporated directly, in vacuum, onto 10 $\mu g/cm^2$ carbon backings mounted on the target ladder. The main target was composed of a 40 $\mu g/cm^2$ layer of enriched (∿ 97%) ^{48}Ca. The remaining two targets, for reasons to be made apparent later, were ^{40}Ca and WO_3. In order that the oxidation of the target be prevented, the ladder was brought up directly into a target vacuum lock system (figure III-1). This system could then be transferred to and fitted over the target chamber. Once the chamber was evacuated, the target ladder could be lowered into it.

Figure III-1

Figure III-1

The target vacuum lock system

The target ladder contained ^{48}Ca, ^{40}Ca, and WO_3 targets. The calcium targets were evaporated, in vacuum, directly onto the ladder as the vacuum lock system was in configuration b). The targets were transferred to the Enge target chamber in configuration a); once the chamber was pumped out, the ladder was lowered into it, forming configuration b).

a)

TARGET VACUUM LOCK SYSTEM

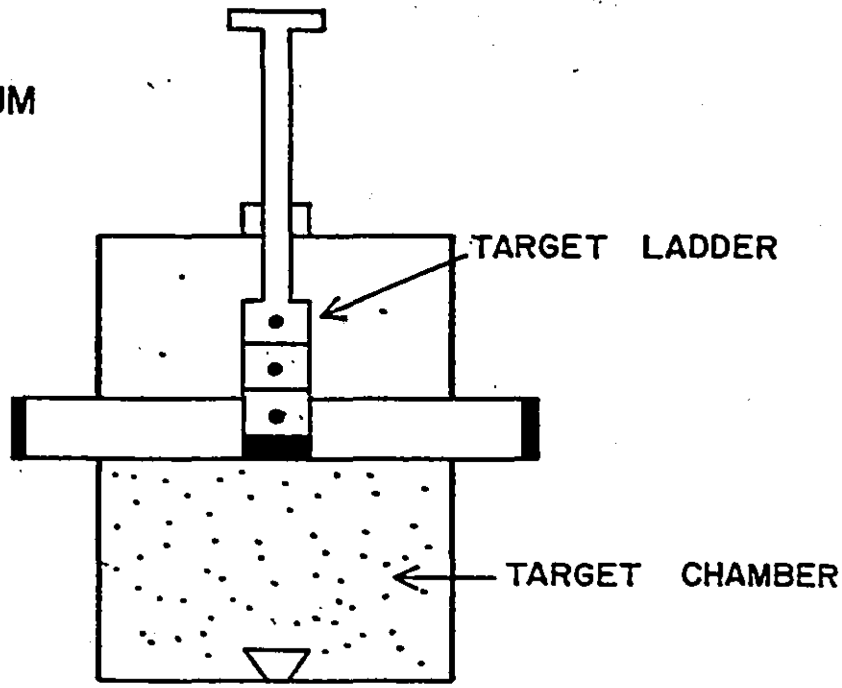

b)

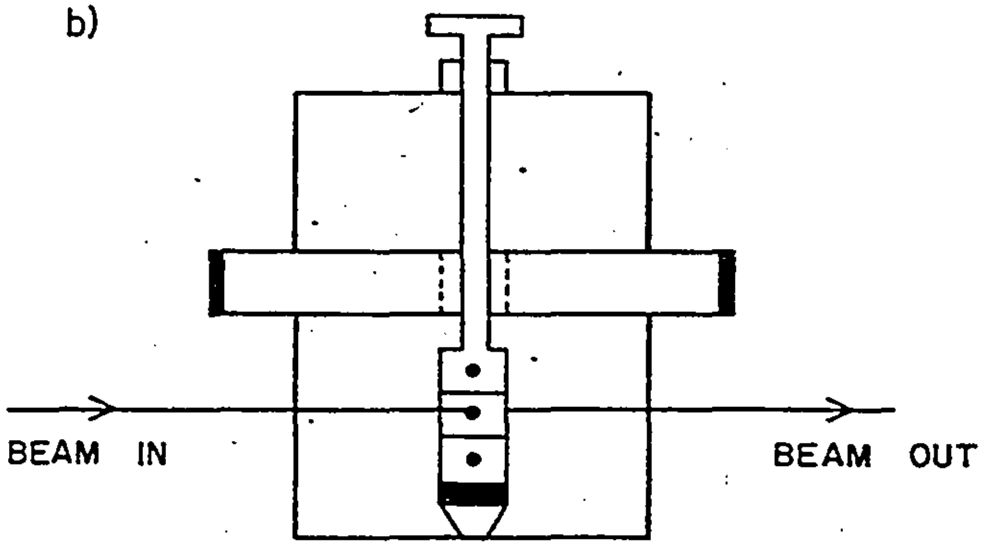

The proportional counter[18,19,20,21] consists of a single nichrome wire inside a chamber filled with a gas mixture of 90% argon and 10% methane. A thin window of aluminized mylar holds the gas in the detector and permits particles to enter with no appreciable loss in energy. A potential of +1000 volts was applied to the anode wire - this is sufficient to cause an electron avalanche once the gas-ionizing reaction products have passed through the counter. Hence, a net charge is built up on the wire in a location corresponding closely to the trajectory of the particle. A flow of current to both ends of the wire then ensues. As the length of the wire is directly proportional to its resistance, a comparison between the voltages of the pulses received at the ends of the wire will yield information as to the location of the original charge buildup. The pulses from the ends of the counter were then put through the rather straightforward coincidence electronics set-up shown in figure III-2. The signals were eventually fed into the PDP-9 computer where a program calculated the charge build-up location and the current position spectrum was then displayed on a CRT screen.

The sum of the pulses from the ends of the counter gave an indication of the energy lost by the particle passing through the front counter. The resulting mass spectrum, essentially a dE/dx spectrum as the particles passed right through, was found to be quite satisfactory in particle identification. Indeed, the alpha particles can be seen to be well resolved from the background deuterons in figure III-3. At smaller angles (less than 4°), these two distinct peaks tended to coalesce. Hence, a window placed on the alpha particle peak would also include some tail-end deuterons resulting in a greater amount of background in the position spectrum. Although a back counter was available to be used in an anti-coincidence mode, it was found to be unnecessary for our purposes.

The distance between the spectrograph magnet and the proportional counter was adjusted to correct for Doppler or kinematic broadening[22] using calculated values. The vertical position of the counter was also adjusted until the maximum count rate was realized.

For each beam energy, runs were performed for deuterons polarized predominately in the m=0 substate and then the m=1 substate. As previously mentioned, the quantization axis can be assumed to be parallel to the beam direction. This process was repeated for each of the three targets. The entire cycle was followed until satisfactory statistics had been obtained. The beam intensities used were in the 15-25 nA range.

III.3 More practical considerations

The detection of alpha particles near 0° tended to run into some difficulties as a result of the presence of the longer range deuterons in the beam. This background

Figure III-2

Figure III-2

A block diagram of the electronics used to process signals from the proportional counter.

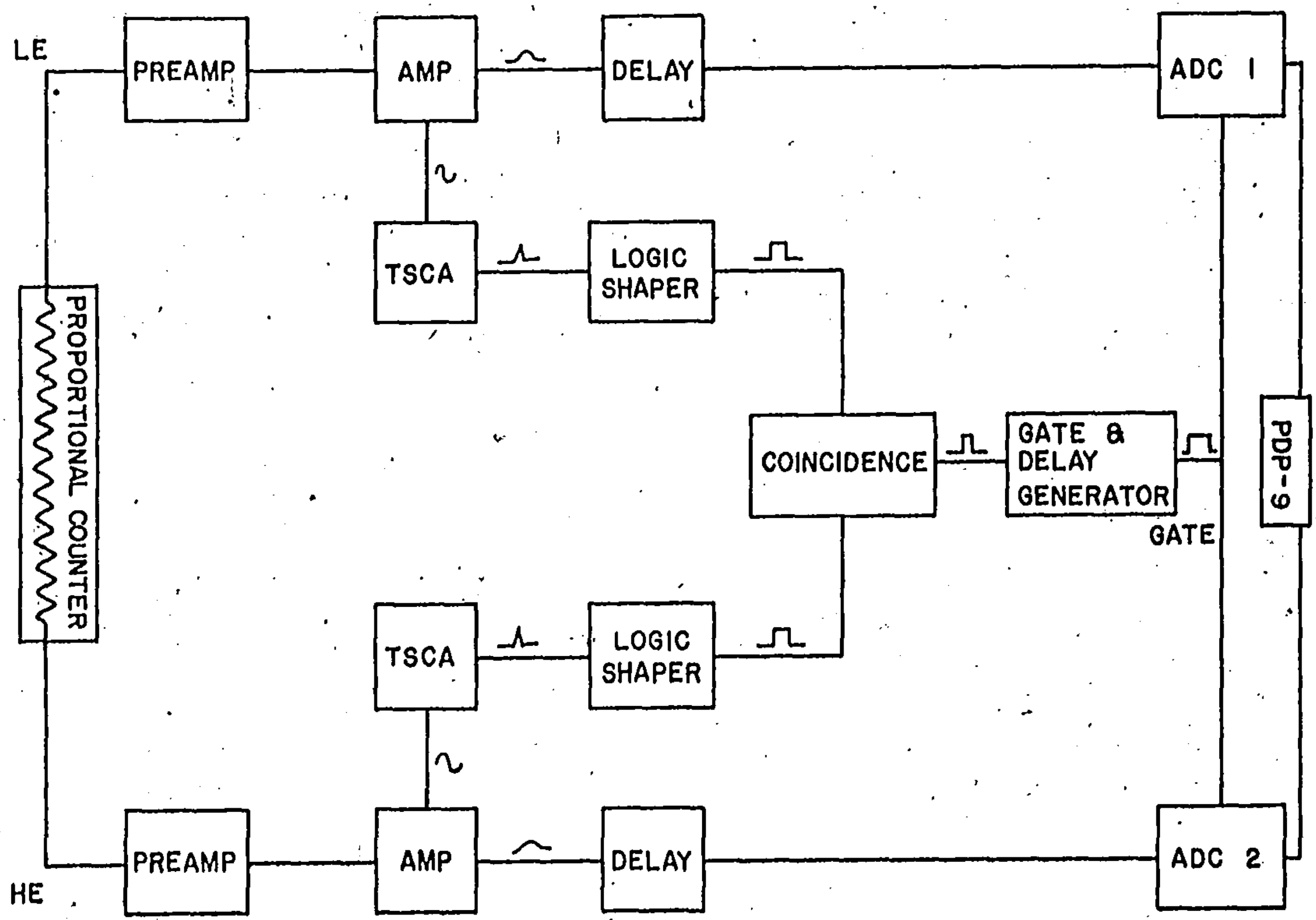
LE
PREAMP
AMP
DELAY
ADC 1
TSCA
LOGIC SHAPER
PROPORTIONAL COUNTER
COINCIDENCE
GATE & DELAY GENERATOR
GATE
PDP-9
TSCA
LOGIC SHAPER
HE
PREAMP
AMP
DELAY
ADC 2

Figure III-3

Figure III-3

The energy loss or mass spectrum from the $^{48}Ca(d,\alpha)^{46}K$ experiment at 4°. Windows were set on the well-resolved alpha particle group to obtain the alpha position spectra shown in Chapter IV.

24(b)

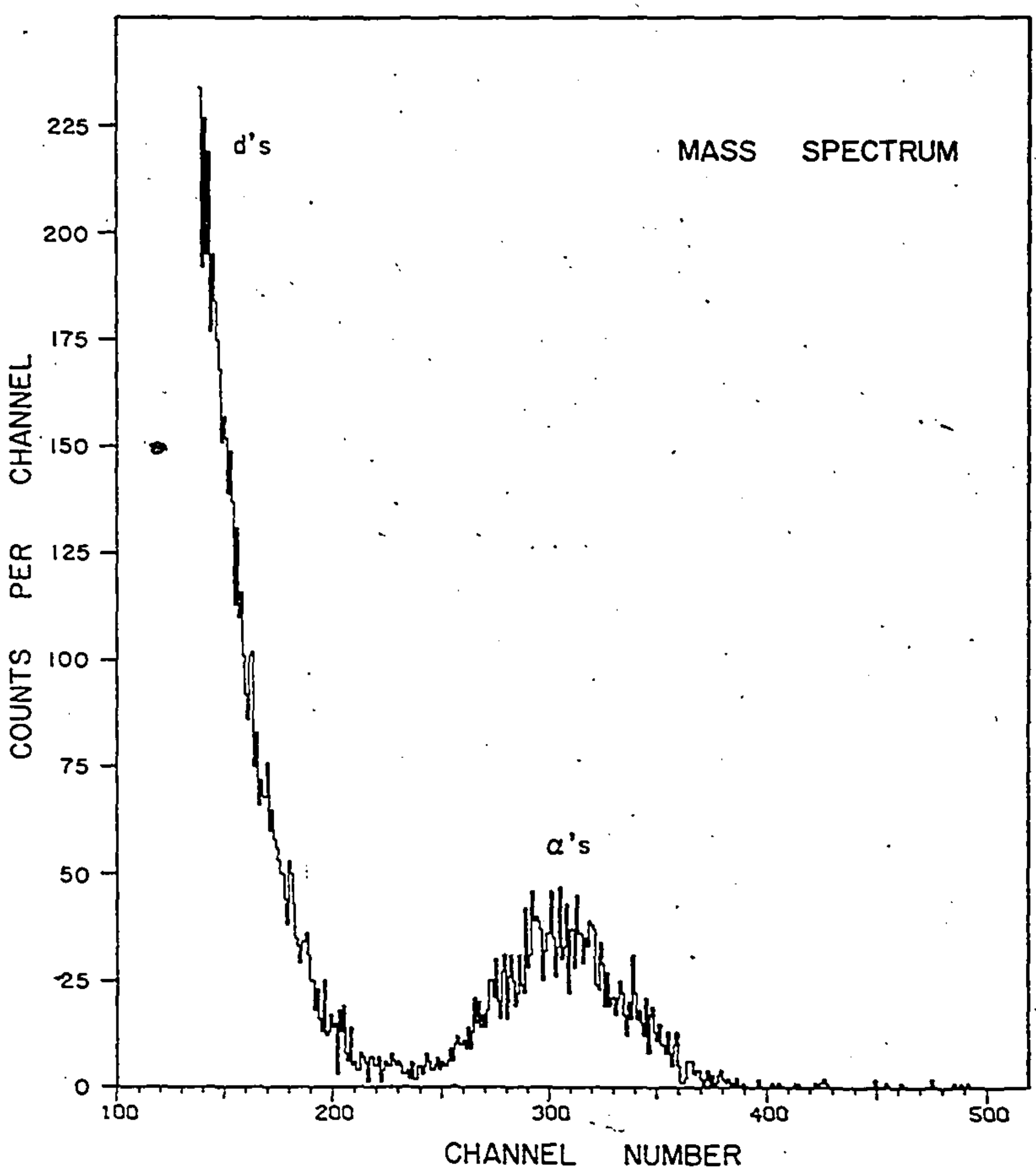

MASS SPECTRUM
d's
α's
COUNTS PER CHANNEL
225
200
175
150
125
100
75
50
25
0
100
200
300
400
500
CHANNEL NUMBER

flux was sufficiently suppressed at 4° so that measurements could be made. However, as a result of not being at 0°, there was a corresponding attenuation of the tensor analyzing power. For a target of ^{40}Ca, 10 MeV deuterons, and $\theta_{cm} = 5°$, Petty[3] estimates an attenuation of 7.6%. In the case of a ^{48}Ca target, the mass increase would probably not be too significant. As lower beam energies and a smaller angle were used, the quoted figure likely over-estimates the attenuation in our experiment somewhat. Nevertheless, it gives some indication of the size of the effect one can expect (perhaps 5-6%).

In practice, a portion of the beam always consists of some unpolarized deuterons. The quench ratio Q is defined as the ratio of the total beam current to the unpolarized component. However, it is often more useful to consider the fractional beam polarization - the ratio of the polarized beam portion to the total beam current. To the first order, it can be connected to the quench ratio by the expression $p = 1 - \frac{1}{Q}$.

By monitoring the quench ratio throughout this experiment, one could ensure that the beam polarization remained fairly constant. The effects of long term variations in the beam polarization were reduced as a result of the switching of the deuteron substate every two to three hours.

The fractional beam polarization was found by measuring the normalized yield ratios for some known natural (and a 0^-) states in $^{14}N^*$. This was produced by a $(\vec{d},\alpha)$ reaction on the tungsten oxide target. A typical set of normalized spectra is shown in figure III-4. Note how the cross-section for the natural parity states at 5.690 and 5.832 MeV is drastically reduced in going from the m=1 to m=0 deuteron substate. It can also be seen that the reverse situation occurs for the 0^- state at 4.915 MeV. As expected, the yield for the remaining unnatural parity states varies in a rather unpredictable fashion. The beam polarization, which remained constant to within ± 5% for any given run, was found to vary anywhere between 50% and 75% over the course of the entire experiment.

Finally, a close examination of figure III-4 shows that a double peak structure is evident for the two ^{10}B levels. A layer of carbon on each side of the target may be responsible. As the WO_3 target is placed on a carbon backing, the deuteron beam must be depositing carbon on the WO_3 surface facing the beam. Energy loss effects due to the passage of the alpha particles through the target would then account for the location of a second alpha peak on the lower energy side of the major alpha peak. The source of this carbon is probably hydrocarbon cracking by the beam in poor vacuum.

Figure III-4

Figure III-4

The position spectra for $^{16}O(\vec{d},\alpha)^{14}N$ with E_d = 7.5 MeV and θ_{lab} = 4°. The top spectrum was for the deuteron beam polarized in the m=1 substate whereas the bottom spectrum was for the m=0 deuteron substate. The fractional beam polarization $\underset{\sim}{p}$ was extracted from the comparison of these two spectra.

27(b)

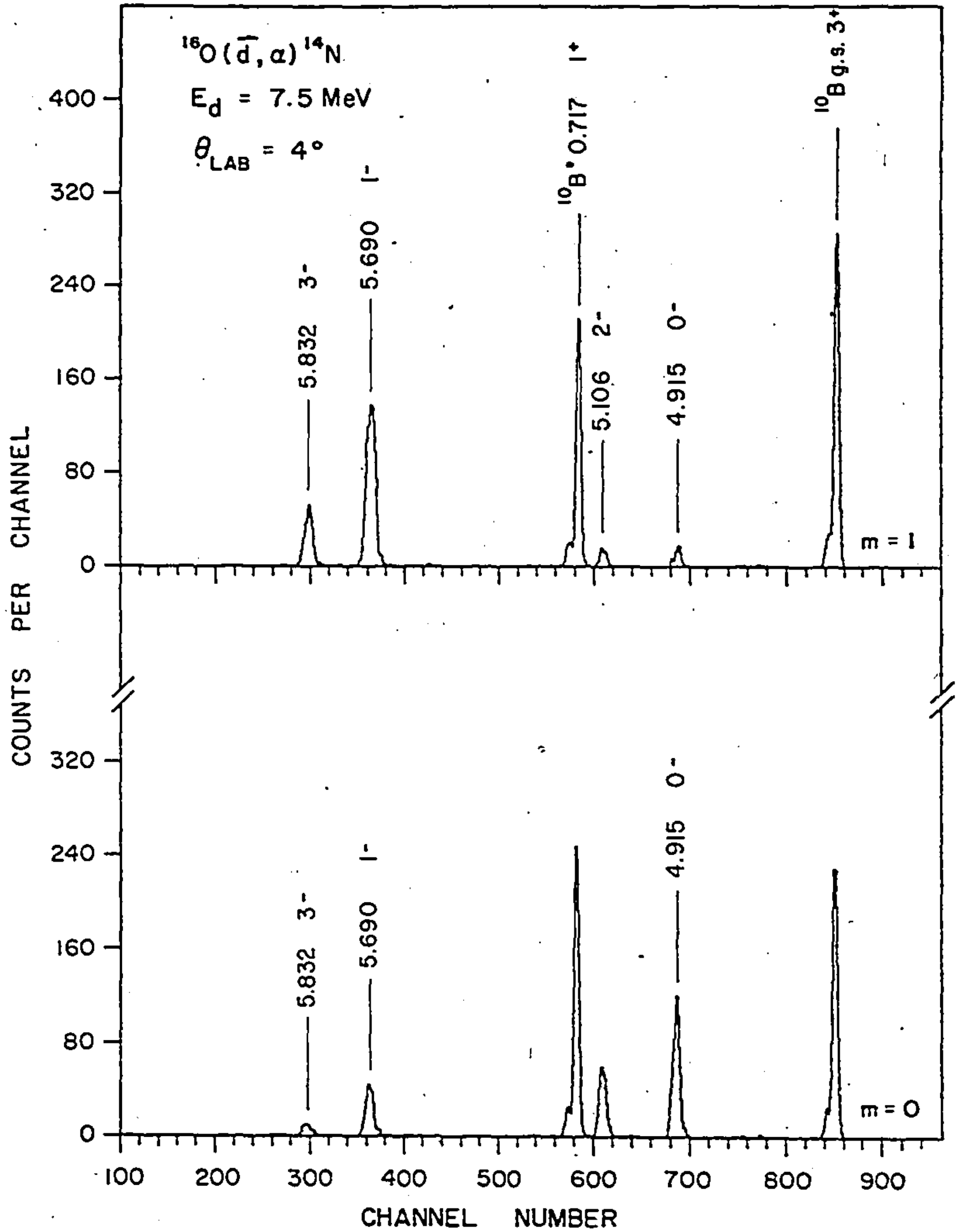

$^{16}O(\vec{d},\alpha)^{14}N$
E_d = 7.5 MeV
θ_{LAB} = 4°
5.832 3-
5.690 1-
$^{10}B^*$ 0.717 1+
5.106 2-
4.915 0-
^{10}B g.s. 3+
m = 1
m = 0
COUNTS PER CHANNEL
CHANNEL NUMBER
0
80
160
240
320
400
100
200
300
400
500
600
700
800
900

CHAPTER IV

EXPERIMENTAL RESULTS

IV.1 Analysis of data

The ^{46}K spectra, labelled with excitation energies obtained from the Nuclear Data Sheets[23], are shown in figures IV-1,2,3,4 for each of the four beam energies used. An attempt was made to measure T_{20} for ^{46}K levels at higher excitation energies, however the resolution obtained together with the background in the spectra rendered the results of little value. In addition, no new levels were found or resolved in the lower region of excitation. Typically, these spectra had a resolution of 20-25 keV FWHM; indeed, a resolution half as good would have been sufficient to separate the ^{46}K peaks in this lower excitation region from each other. The main cause for concern was due to the interference of impurity peaks from ^{38}K contaminants. The Q value for a (d,α) reaction on ^{40}Ca is such that one observes the 3-5 MeV excitation region of the odd-odd final nucleus ^{38}K; thus, a high density of states is witnessed. The cross-section for this reaction was at least an order of magnitude greater than for $^{48}Ca(d,\alpha)^{46}K$. As a result, this problem was present even though a highly enriched target was used. The reasons for the much larger cross-sections for the ^{40}Ca target will now be discussed.

Figure IV-1

Figure IV-1

Energy spectra of α particles from the $^{48}Ca(\vec{d},\alpha)^{46}K$ reaction (m=0/m=1) at $\theta_{lab} = 4°$ for a deuteron beam energy of 7.5 MeV. The major target contaminant levels, labelled in the m=1 spectrum, result from $(\vec{d},\alpha)$ reactions on ^{28}Si, ^{24}Mg, ^{16}O, and ^{13}C.

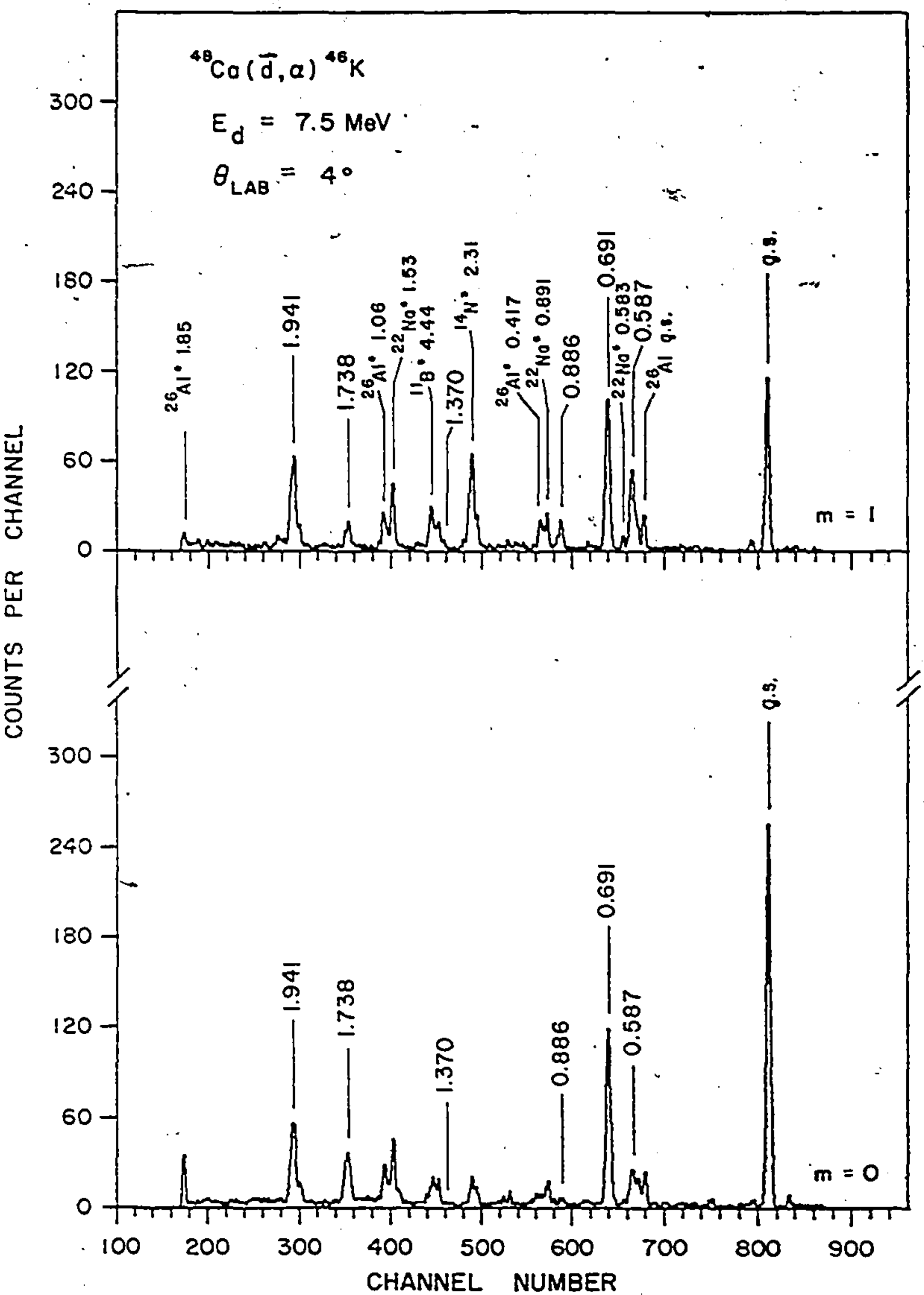

$^{48}Ca(\vec{d},\alpha)^{46}K$
E_d = 7.5 MeV
θ_{LAB} = 4°
COUNTS PER CHANNEL
CHANNEL NUMBER
m = 1
m = 0
g.s.
0.691
0.587
0.886
1.370
1.738
1.941
$^{26}Al^*$ 1.85
$^{26}Al^*$ 1.06
$^{22}Na^*$ 1.53
$^{11}B^*$ 4.44
$^{14}N^*$ 2.31
$^{26}Al^*$ 0.417
$^{22}Na^*$ 0.891
$^{22}Na^*$ 0.583
^{26}Al g.s.

Figure IV-2

Figure IV-2

Energy spectra of α particles from the $^{48}Ca(\vec{d},\alpha)^{46}K$ reaction (m=0/m=1) at θ_{lab} = 4° for a deuteron beam energy of 8.0 MeV.

30(b)

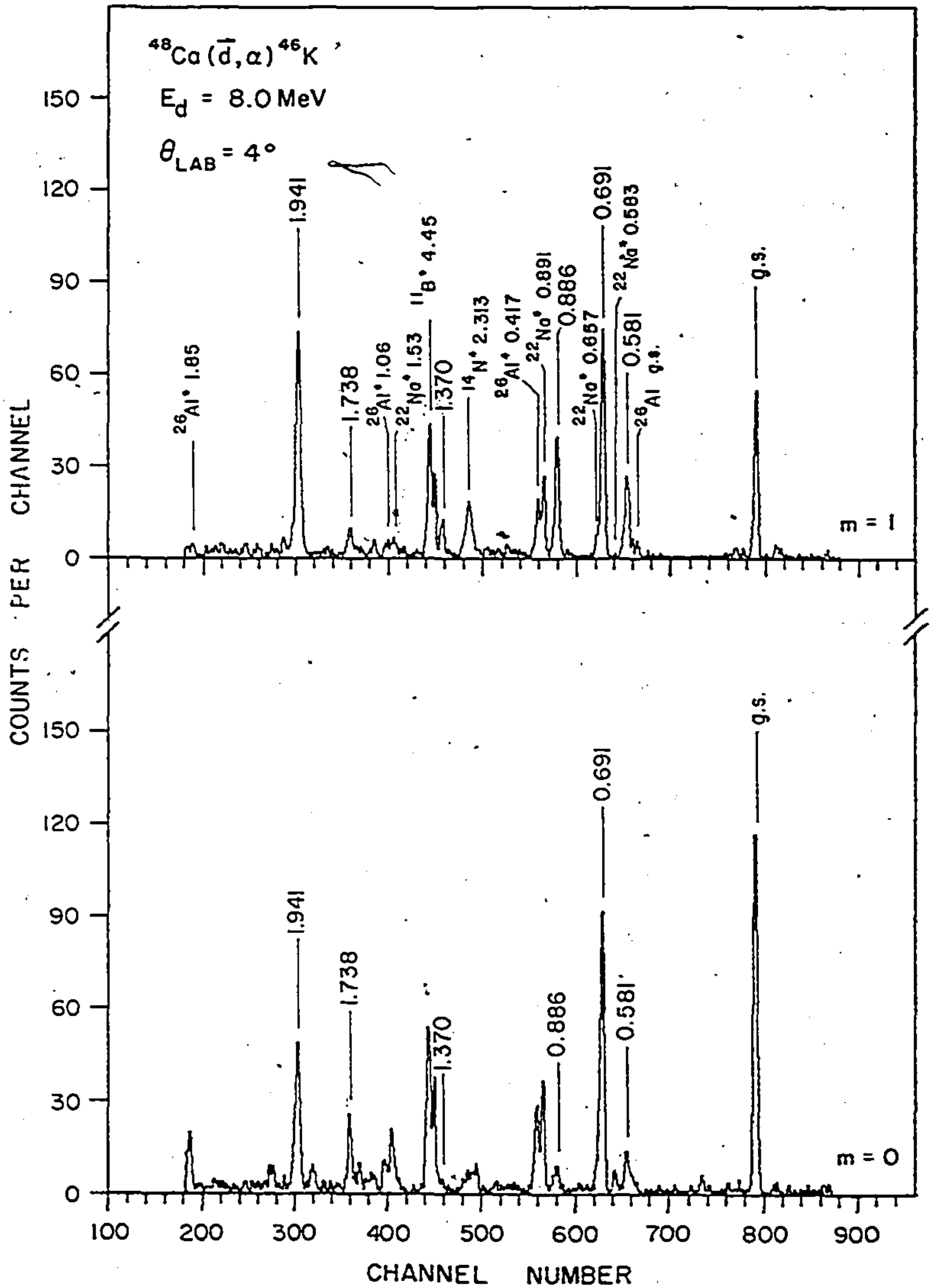

$^{48}Ca(\vec{d},\alpha)^{46}K$
E_d = 8.0 MeV
θ_{LAB} = 4°
COUNTS PER CHANNEL
CHANNEL NUMBER
m = 1
m = 0
1.941
1.738
1.370
0.886
0.691
0.581
g.s.
$^{26}Al^*$ 1.85
$^{26}Al^*$ 1.06
$^{22}Na^*$ 1.53
$^{11}B^*$ 4.45
$^{14}N^*$ 2.313
$^{26}Al^*$ 0.417
$^{22}Na^*$ 0.891
$^{22}Na^*$ 0.657
$^{22}Na^*$ 0.583
^{26}Al g.s.

Figure IV-3

Figure IV-3

Energy spectrum of α particles from the $^{48}Ca(\vec{d},\alpha)^{46}K$ reaction (m=0/m=1) at $\theta_{lab} = 4°$ for a deuteron beam energy of 8.5 MeV. A failure of the polarized ion source terminated this experiment before satisfactory statistics had been obtained.

31(b)

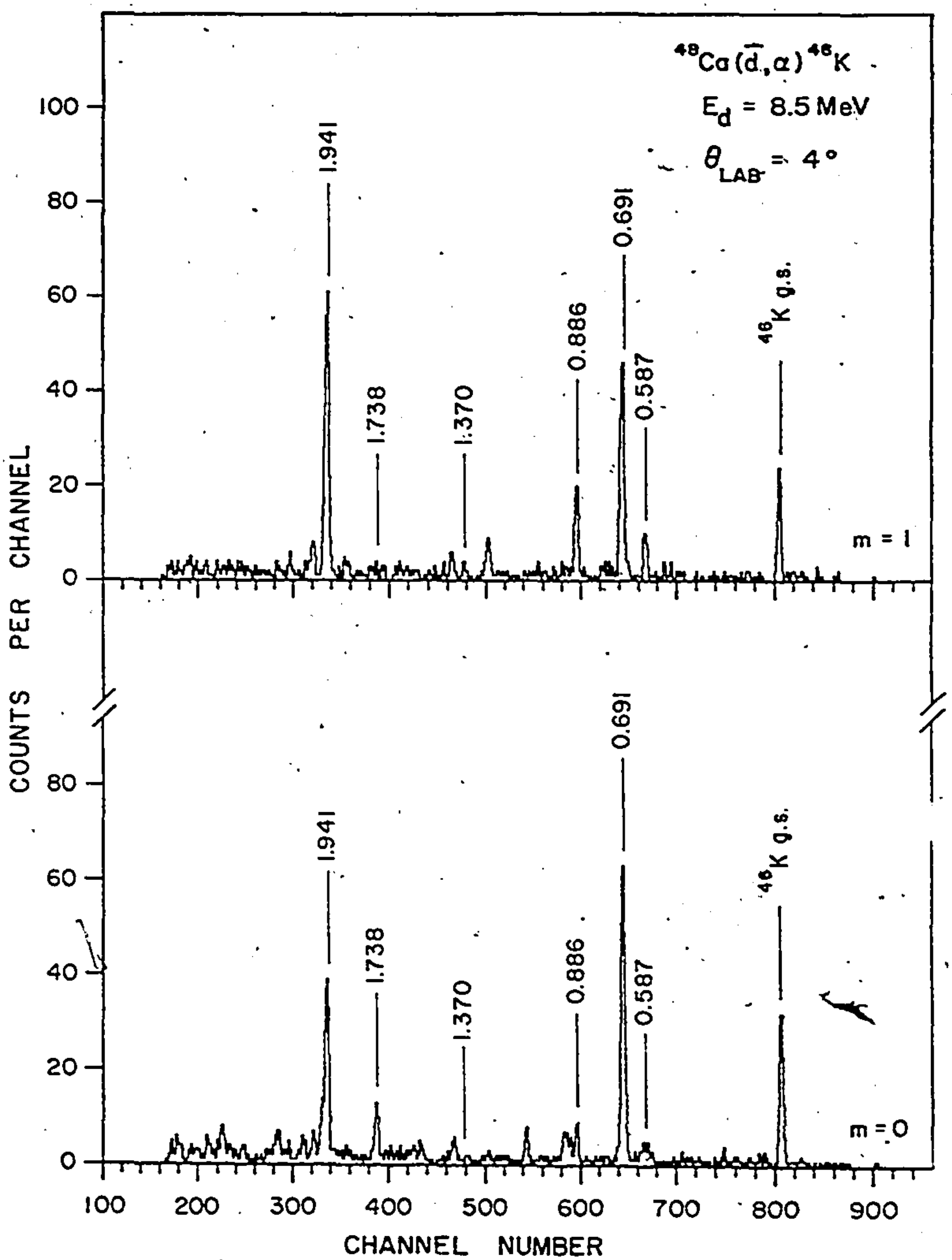

$^{48}Ca(\vec{d},\alpha)^{46}K$
E_d = 8.5 MeV
θ_{LAB} = 4°
1.941
1.738
1.370
0.886
0.691
0.587
^{46}K g.s.
m = 1
m = 0
COUNTS PER CHANNEL
CHANNEL NUMBER

Figure IV-4

Figure IV-4

Energy spectra of α particles from the $^{48}Ca(\vec{d},\alpha)^{46}K$ reaction (m=0/m=1) at θ_{lab} = 4° for a deuteron beam energy of 9.0 MeV.

32(b)

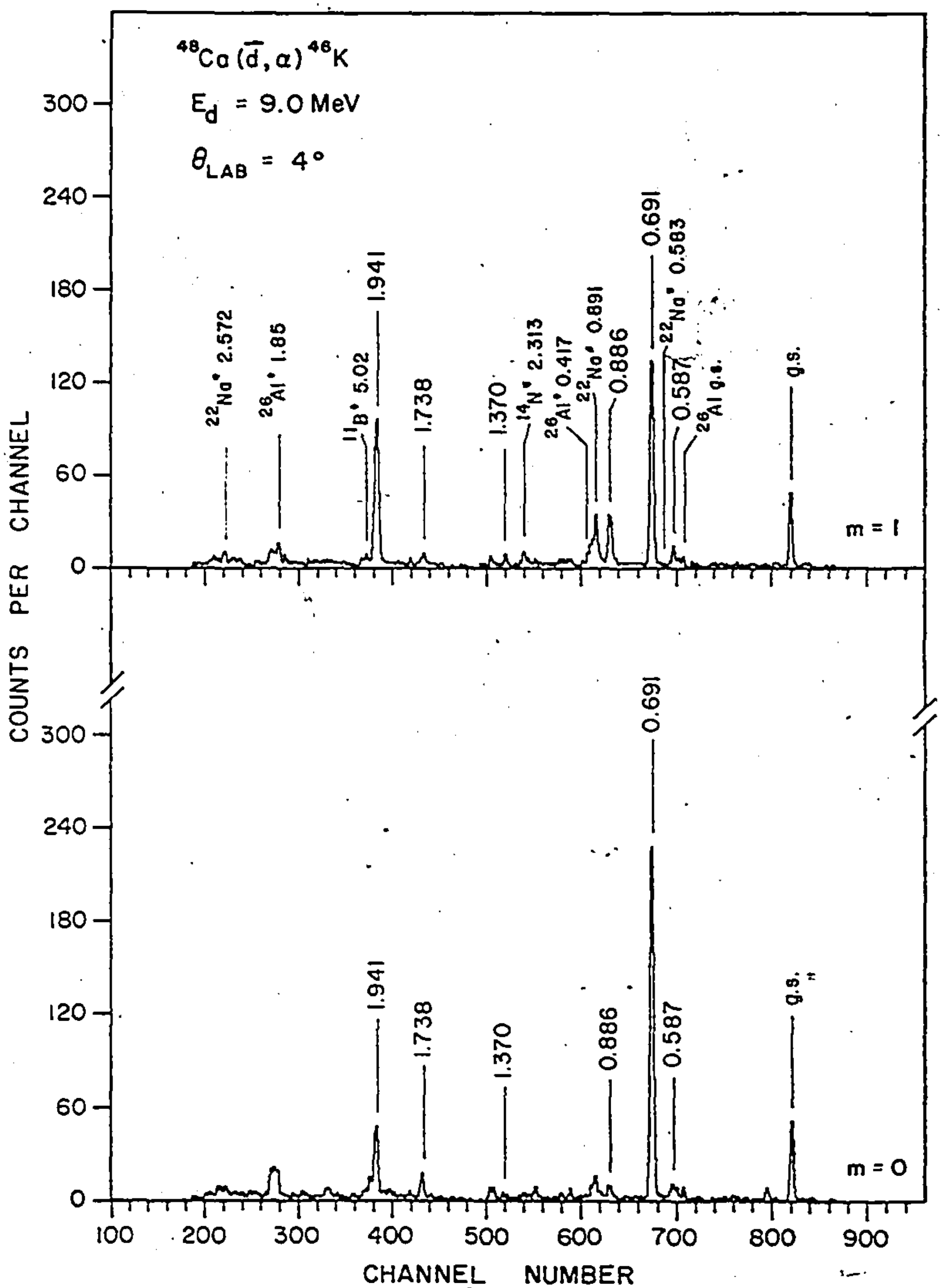

$^{48}Ca(\bar{d},\alpha)^{46}K$
E_d = 9.0 MeV
θ_{LAB} = 4°
$^{22}Na^*$ 2.572
$^{26}Al^*$ 1.85
$^{11}B^*$ 5.02
1.941
1.738
1.370
$^{14}N^*$ 2.313
$^{26}Al^*$ 0.417
$^{22}Na^*$ 0.891
0.886
0.691
$^{22}Na^*$ 0.583
0.587
^{26}Al g.s.
g.s.
m = 1
m = 0
COUNTS PER CHANNEL
CHANNEL NUMBER

It has been observed empirically that the largest cross-sections for both (d,α)[24] and (α,d)[25,26] reactions tend to occur when the transferred proton and neutron are coupled to maximum J and are acquired from the same shell. The selectivity of the (d,α) reaction was mentioned in chapter II. In addition, a further selectivity exists depending upon how well these two nucleons are correlated in the nucleus. Both angular momentum coupling and attractive nucleon-nucleon forces are responsible for this correlation[5]. The latter ingredient can be described by configuration-mixed wavefunctions.

Glendenning[5] outlines a classical physics analogy for angular momentum coupling correlations. If the two particles are coupled to a total angular momentum J, then the classical orbits of such particles in the nucleus are coplanar only when J assumes its maximum or minimum values. For any intermediate values, the two orbits are inclined with respect to each other. Thus, it can be seen that a higher degree of spatial correlation exists in the first case.

The low lying states of the nuclei ^{38}K and ^{46}K may be described, on the basis of the shell model, as a neutron hole and a proton hole in ^{40}Ca and ^{48}Ca cores, respectively. The expected ground state configurations would be $\pi d_{3/2}^{-1}\nu d_{3/2}^{-1}$ for ^{38}K and $\pi d_{3/2}^{-1}\nu f_{7/2}^{-1}$ for ^{46}K. In the case of ^{38}K the nucleon pair could be captured from the same shell as a unit in a direct reaction. The neutron and proton are in a relative s-state so that there would be a great deal of overlap between their radial wavefunctions; consequently, the final state in the alpha particle parallels the initial state. For ^{46}K, however, as the proton and neutron are apparently from different shells, it is possible that the reaction may be proceeding through some multi-step process (perhaps in competition with a direct transfer reaction).

If one assumes a compound nuclear reaction instead, the instability of the neutron-rich ^{46}K nucleus can explain the discrepancy in the cross-sections[14]. Using such a model, a deuteron incident upon a ^{40}Ca (or ^{48}Ca) target will produce an excited ^{42}Sc (or ^{50}Sc) compound nucleus. For the case of a ^{42}Sc compound nucleus, an examination of Q value tables reveals that only the proton channel opens sooner than the alpha channel. As a result, a decay by alpha emission should be quite probable. Alternatively, because of the large neutron excess in ^{50}Sc, one would expect neutrons to be expelled rather easily; indeed, it turns out to be favourable in terms of energy and the fact that there is no Coulomb barrier for neutrons. Both neutron and proton channels open sooner than the alpha channel. As a result of the availability of the neutron channels, the alpha decay of the ^{50}Sc compound nucleus will be inhibited in comparison to the ^{42}Sc

Figure IV-5

Figure IV-5

A normalized ^{38}K spectrum is compared with an uncorrected ^{46}K spectrum for 7.5 MeV deuterons in the m=0 substate. The insert gives a magnified view of the dotted regions superimposed over each other; here, the ^{38}K spectrum is shaded in for greater visibility.

35(b)

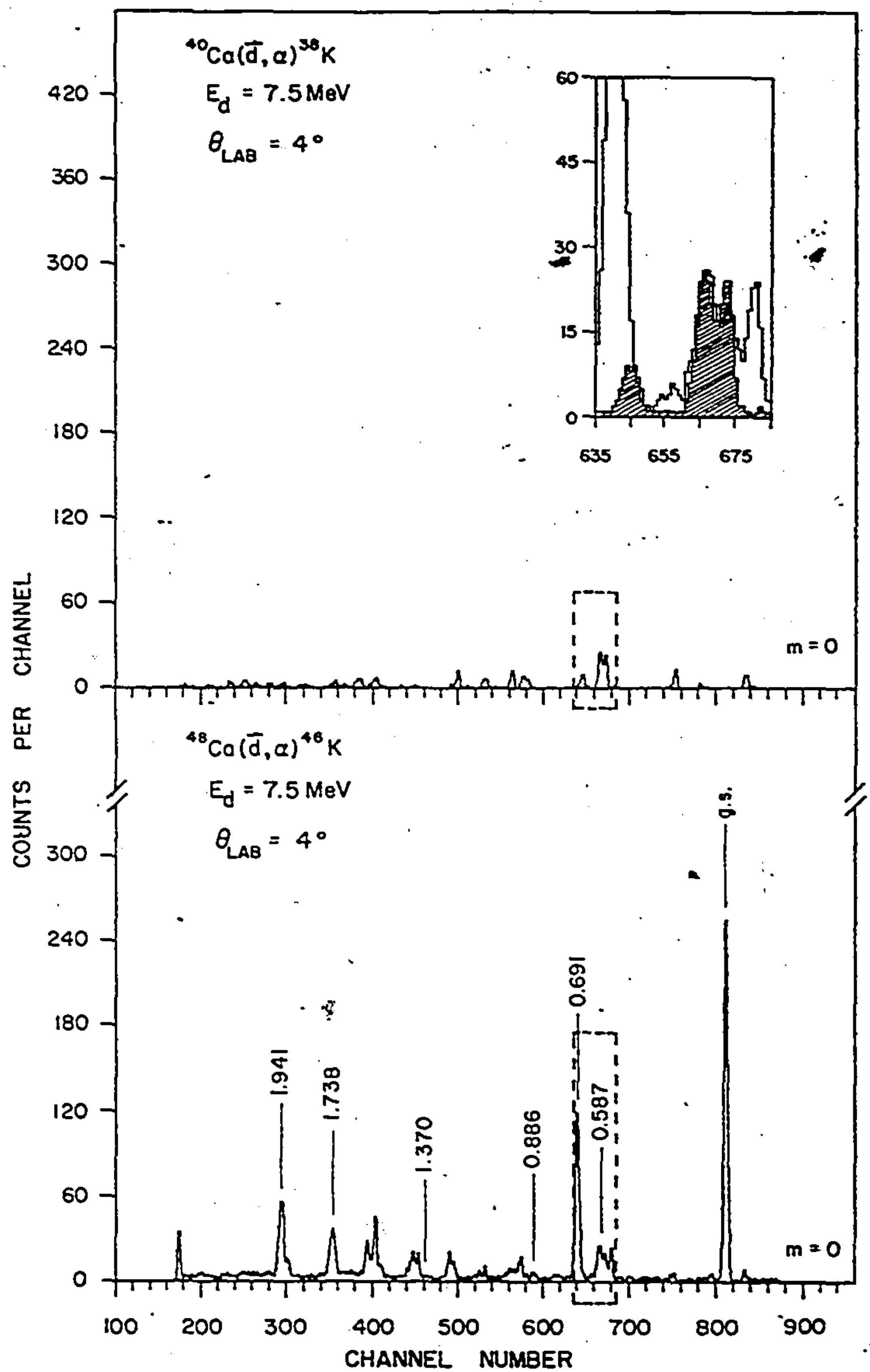

$^{40}Ca(\vec{d},\alpha)^{38}K$
E_d = 7.5 MeV
θ_{LAB} = 4°
m = 0
$^{48}Ca(\vec{d},\alpha)^{46}K$
E_d = 7.5 MeV
θ_{LAB} = 4°
1.941
1.738
1.370
0.886
0.691
0.587
g.s.
m = 0
COUNTS PER CHANNEL
CHANNEL NUMBER

Figure IV-6

Figure IV-6

A normalized ^{38}K spectrum is compared with an uncorrected ^{46}K spectrum for 7.5 MeV deuterons in the m=1 substate. The insert gives a magnified view of the dotted regions superimposed over each other; here, the ^{38}K spectrum is shaded in for greater visibility.

366

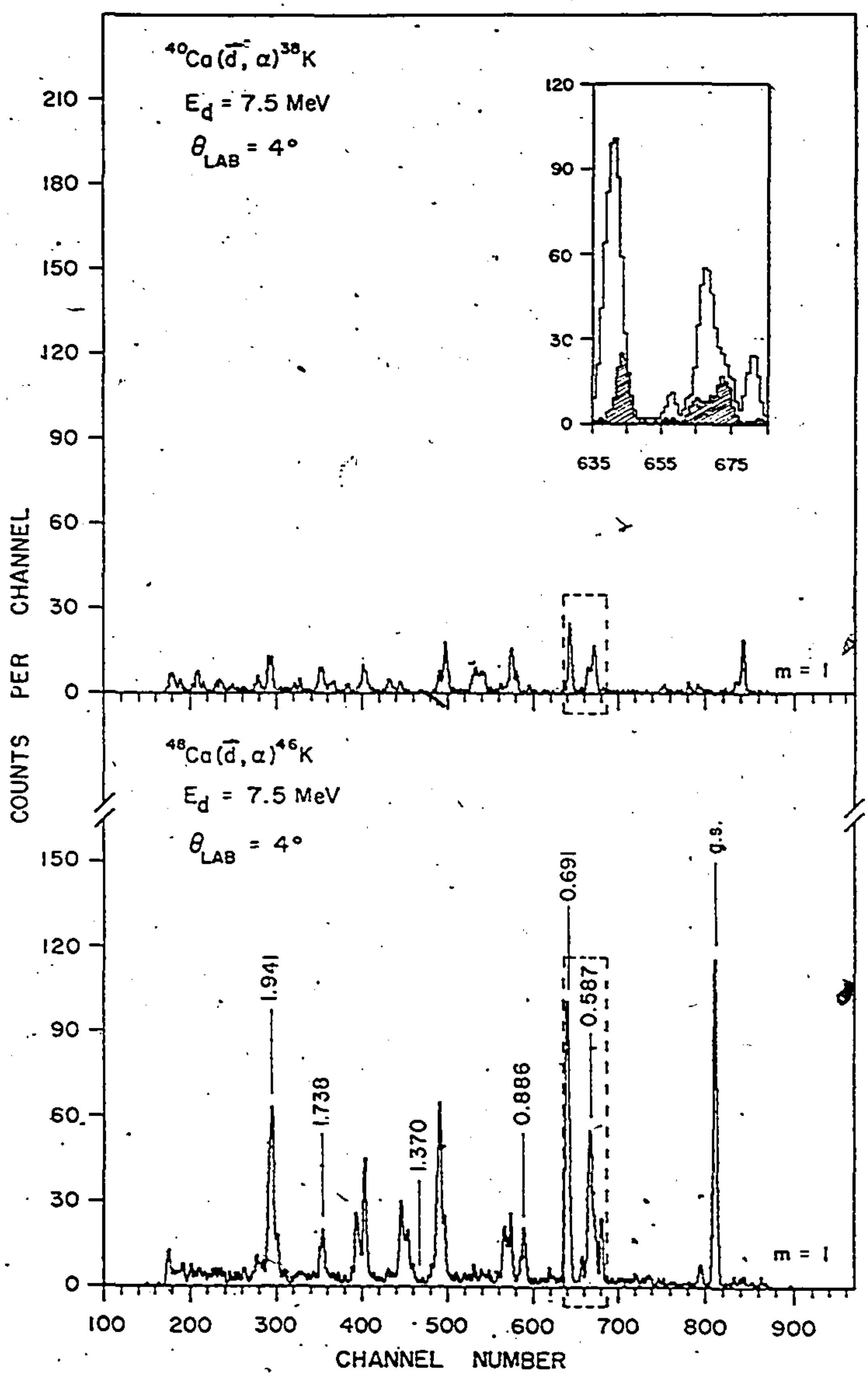

$^{40}Ca(\vec{d},\alpha)^{38}K$
E_d = 7.5 MeV
θ_{LAB} = 4°
m = 1
$^{48}Ca(\vec{d},\alpha)^{46}K$
E_d = 7.5 MeV
θ_{LAB} = 4°
1.941
1.738
1.370
0.886
0.691
0.587
g.s.
m = 1
COUNTS PER CHANNEL
CHANNEL NUMBER

nucleus. Both compound nuclear and direct reaction mechanisms indicate that the (d,α) cross-sections for ^{46}K should be weaker than those for ^{38}K; this is, in fact, what is observed.

To correct for these impurity peaks, a ^{38}K spectrum, for each of the m=0 and m=1 deuteron beam substates was taken during each cycle. The spectra were normalized by comparing ^{38}K impurity peaks in the ^{46}K spectrum with the corresponding peaks in ^{38}K spectra and they were then subtracted. An example is given in figures IV-5,6. The resulting m=0/m=1 ^{46}K spectra for a given beam energy were then normalized according to the number of beam dumps recorded from charge integration of the Faraday cup.

The tensor analyzing powers T_{20} were calculated as outlined in chapter II and are plotted against the excitation energy of ^{46}K levels in figure IV-7. For a given state in this diagram, T_{20} is plotted from left to right for beam energies corresponding to 7.5, 8.0, 8.5 and 9.0 MeV respectively. The error range shown for each point reflects:

a) the uncertainty in the beam polarization

b) the statistical uncertainty in the peak intensities and

c) the estimated uncertainty in the normalization of the correction ^{38}K spetra.

IV.2 Parity assignments and comparison with published results

A summary of the results from this experiment is given in table IV-1. The T_{20} values at $\theta_{lab} = 4°$ are averaged over the beam energy and a corresponding assignment of the parity of the level is made (unnatural U or natural N). The excitation energies ~~and~~ adopted J^{π} and L assignments were obtained from the Nuclear Data Sheets[23].

As mentioned in the introduction, only three basic types of experiments have been reported in the literature to obtain ^{46}K spectra:

(i) Angular distributions of (d,α) reactions were used to deduce L assignments by Orloff and Daehnick[27], Daehnick et.al.[1,2] and Paul et.al.[28]. These L assignments were then used to deduce J and π in some cases.

(ii) Another approach used was to obtain angular distributions of $(p,{}^{3}He)$ reactions and to compare these with T=4 analog states in ^{46}Ca from (p,t) reactions. Distorted wave Born approximation (DWBA) calculations were carried out for the latter distributions which lead to L and, ultimately, J^{π} assignments. This procedure was followed by Dupont et.al.[29,30] and Daehnick and Sherr[31].

(iii) Finally, γ ray transitions were observed in (d,αγ) coincidence experiments by Daehnick et.al.[1,2].

The individual levels will now be discussed. The first line for each state will give the excitation energy,

Figure IV-7

Figure IV-7

The tensor analyzing powers T_{20} are plotted as a function of the excitation energy E* of levels in ^{46}K. For a given state in this chart, T_{20} is plotted from left to right for beam energies corresponding to 7.5, 8.0, 8.5, and 9.0 MeV respectively. The limits for natural parity ($T_{20} = +\frac{1}{\sqrt{2}}$) and $J^{\pi} = 0^{-}$ ($T_{20} = -\sqrt{2}$) are indicated by the dotted lines and the final parities are listed along the top of the diagram. Note that for E* = 1.370 MeV, there is no point available for a beam energy of 8.5 MeV.

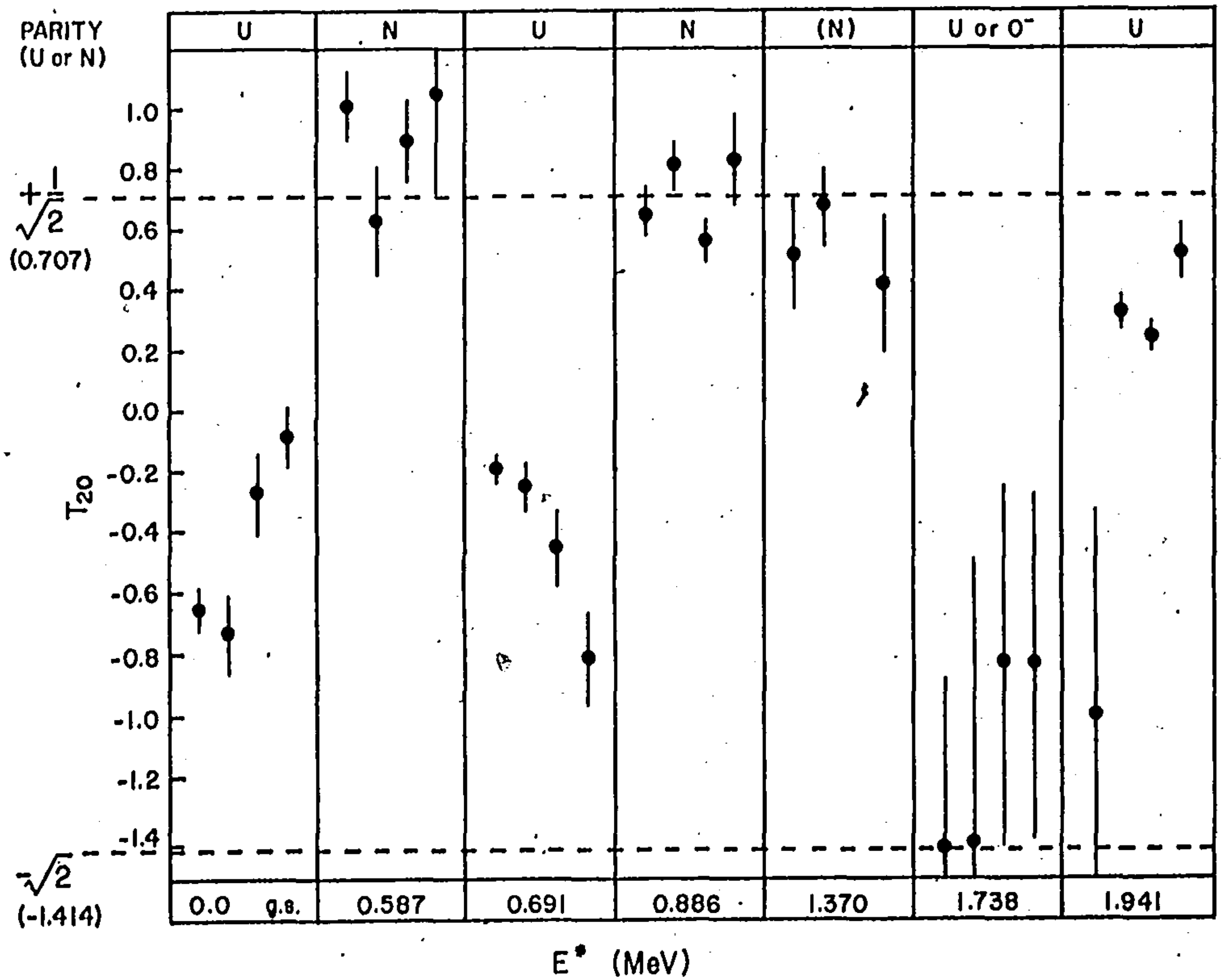

PARITY (U or N)
U
N
U
N
(N)
U or O⁻
U
1.0
0.8
0.6
0.4
0.2
0.0
-0.2
-0.4
-0.6
-0.8
-1.0
-1.2
-1.4
T20
+1/√2 (0.707)
-√2 (-1.414)
0.0 g.s.
0.587
0.691
0.886
1.370
1.738
1.941
E* (MeV)

39b

most recent spin and parity assignment J^{π}, and the parity (U or N) determined from this experiment.

(0) ground state E* = 0.00 MeV $J^{\pi} = 2^{-}$ U.

All previous experimental evidence is consistent with this assignment. The spin and parity is predicted by the Nordheim strong rule if one assumes a $\pi d^{-1}_{3/2} \nu f^{-1}_{7/2}$ ground state configuration. This peak has one of the larger cross-sections in the ^{46}K spectrum.

Prior measurements indicated an unnatural parity for this level (as well as for the 0.691 and 1.941 MeV states) due to the fact that (p,t) transitions were attenuated by at least an order of magnitude in comparison to the corresponding (p,^{3}He) levels. The angular distribution is well fitted by a mixture of an L=1 distorted wave curve and an empirical L=3 curve[31]. This leads to the choice of $J^{\pi} = 2^{-}$. The results in figure IV-7 agree that this is indeed an unnatural parity state, adding further weight to this assignment.

(1) E* = 0.587 MeV $J^{\pi} = 3^{-}$ N

Paul et.al.[28] assigned $J^{\pi} = 4^{-}$ to this level, but all other results agree with the one given above. Paul compared angular distributions from ^{46}K with ^{40}K to obtain his L values. Daehnick and Sherr[31] have suggested that for the beam energy used (11 MeV) compound nuclear contributions are significant and may have varied from one isotope

Table IV-1

^{46}K adopted levels from the Nuclear Data Sheets (ref. 23)

E* (MeV)	J^{π}	$L^{\surd\surd}$	$\langle T_{20} \rangle$ (at 4°)	our parity unnatural U or natural N
0.000	(2−)	(1+3)	−0.44±0.06	U
0.587	(3−)	3	+0.89 ±0.11	N
0.691	(4−)	(3+5)	−0.44±0.05	U
0.886	(5−) $\surd\surd\surd$	5	+0.71±0.05	N
1.370	(3−)	3	+0.54±0.12 $\surd$	(N)
1.738	−	(3)	−1.12±0.33	U
1.941	(1+)	(0+2)	+0.03±0.17	U
2.222 $\surd\surd\surd$	(0+) $\surd\surd\surd$	0 $\surd\surd\surd$	−	−
2.790 $\surd\surd\surd$	(2+) $\surd\surd\surd$	(2) $\surd\surd\surd$	−	−
2.969 $\surd\surd\surd$	(4−) $\surd\surd\surd$	(3+5) $\surd\surd\surd$	−	−

$\surd$ averaged only over 7.5, 8.0, and 9.0 MeV

$\surd\surd$ from (d,α) unless otherwise indicated

$\surd\surd\surd$ from ^{48}Ca(p,^{3}He).

The excitation energies shown are known to 6 keV or better.

to another, thereby making these L assignments suspect. Fairly reliable DWBA fits for L=3 have been made for this level giving the above result. Certainly, our results agree with the latter interpretation. As this level suffered the most interference from ^{38}K and had a relatively small cross-section, it is not surprising to see some of the T_{20} values on the high side.

(2) $E^* = 0.691$ MeV $J^\pi = 4^-$ U.

An assignment of $J^\pi = 5^-$ to this level made by Paul et.al.[28] is again discredited by our results. All other measurements have suggested $J^\pi = 4^-$ agreeing with our unnatural parity assignment. In particular, γ-ray cascades from the 0.886 to 0.691 to 0.587 MeV states strongly suggest J=4 for this level. This state also has one of the larger yields in this spectrum.

(3) $E^* = 0.886$ MeV $J^\pi = 5^-$ N.

Paul et.al.[28] have suggested $J^\pi = 3^-$ for this state which cannot be refuted by our natural parity assignment. However, excellent fits by L=5 curves have been made, by others, to the angular distribution thereby providing the result given above.

(4) $E^* = 1.370$ MeV $J^\pi = 3^-$ (N).

Dupont et.al.[30] was not able to distinguish between 3^- or 4^- for this state but Daehnick[2,31] claims a $J^\pi = 3^-$ assignment using angular distributions from (p,^{3}He) and (d,α) reactions. Only three energies were used in our results because of poor statistics. Due to the rather weak excitation of this level only a tentative assignment of natural parity can be made.

(5) $E^* = 1.738$ MeV $J^\pi = 4^-$ U or 0^-

This level is believed to have been populated by non-direct reactions and was assigned this spin and parity on the basis of (d,α) data and shell model arguments[2]. The energy and cross-section for this state seem to be almost correct for a second 4^- state as will be explained in the next chapter. The assignment obtained in this experiment implies that the state is either 0^- (within error limits) or has unnatural parity. The fact that a γ decay has been observed between this level and the 0.587 MeV level (3^-) by Daehnick et.al. lends support to the assignment of $J^\pi = 4^-$ to the 1.738 MeV state. The fast coincidence electronics used should have been able to detect E1, M1, or E2 transitions (i.e. $t_{1/2} << 10^{-7}$ sec.)[2]. A $J^\pi = 0^-$ assignment to this state, on the other hand, would raise the unlikely possibility than an M3 transition was observed. One would expect more favourable transitions to be detected such as an E1 transition (1.941 MeV (1^+) to 1.738 MeV (0^-?)) or an E2 transition (1.738 MeV (0^-?) to the ground state (2^-)). Hence, the 0^- possibility can probably be discarded in favour of an assignment of unnatural parity.

(6). $E^* = 1.941$ MeV $J^\pi = 1^+$ U.

This level has been assigned $J^\pi = 4^-$ by Dupont et. al.[29,30], $J^\pi = 3^-$ by Daehnick et.al.[1], and $J^\pi = 1^+$ by Daehnick et.al.[2,31]. The middle alternative can be ruled out by our results. The most recent DWBA L = 0+2 fits by the latter reference plus the fact that γ decays occur exclusively to the ground state from this level strongly supports the $J^\pi = 1^+$ assignment. This level also had a large cross-section in this spectrum.

Daehnick and Sherr[31] have reported three additional ^{46}K states in this lower excitation region: $E^* = 2.22$ MeV $J^\pi = (0^+)$, $E^* = 2.79$ MeV $J^\pi = (2^+)$, $E^* = 2.97$ MeV $J^\pi = (4^-)$ (believed to have been a candidate for the second 4^- level mentioned in the introduction). While the levels were barely discernible from the background in the ^{46}K spectrum, they were more readily visible as the analog states in ^{46}Ca. The data were not as complete as for the previous states nor were the DWBA L curve fits as good. Of course, equation (13) rules out the observation of the $E^* = 2.22$ MeV level in our experiment providing the $J^\pi = 0^+$ assignment is correct. Neither of the other two states could be distinguished from the background in the ^{46}K spectrum.

Both the ground state and 0.691 MeV level contain higher admixtures of L=3 (with L=1) and L=5 (with L=3), respectively (refer to table IV-1). These admixtures are permitted by the selection rules, but the observed magnitudes can only be explained if there is a perceptible two step transfer. In the work quoted above, it was assumed that the two step transfer did not significantly alter the angular distribution (i.e. the assignments were model dependent to a certain extent)[2].

It should also be mentioned that the DWBA calculations do not predict the finer details too well; some confusion may result as to which L value can be assigned. In addition, the choice of optical-model parameters must be done carefully, as the calculated angular distributions are quite sensitive to this.

CHAPTER V

CALCULATIONS AND DISCUSSION

V.1 Pandya calculations

The energy levels of a nucleon-hole system can be related to the energy levels of the corresponding nucleon-nucleon system by applying a theorem first developed by Pandya[32]. This method does not rely upon any characteristics of the two nucleon interaction as it is included empirically; however, it does assume jj coupling between the proton particle (or hole) and neutron particle (or hole). The latter assumption of jj coupling provides a good description of the low-lying nuclear states in the region of the $1f_{7/2}$ shell. Pandya's theorem can be expressed as:

$$E_J(j^{-1}j') = - \sum_{J_0} (2J_0+1)W(jj'j'j;JJ_0)E_{J_0}(jj') + C \quad (25)$$

where the proton hole (or particle) in shell j and the neutron hole (or particle) in shell j' are coupled together to form a spin J, W(abcd;ef) is the Racah coefficient and C is a constant chosen so that $E_{J_{g.s.}} = 0$ MeV (i.e. $J_{g.s.}$ is simply the spin of the ground state level). The summation is carried out over all possible values J_0 arising from jj coupling between the j shell and j' shell.

Pandya[32] used this theorem to calculate the energy levels for $^{38}Cl(\pi d_{3/2}\nu f_{7/2})$ from the $^{40}K(\pi d_{3/2}^{-1}\nu f_{7/2})$ levels. The results from such calculations are presented in table V-1. The measured excitation energies[33] agree amazingly well with the calculated values - within 25 keV. It should also be mentioned that similar results were obtained independently by Goldstein and Talmi[34] by using the numerical values for the coefficients of fractional parentage and not Pandya's theorem directly. Nevertheless, both methods actually invoke the same assumptions and follow essentially parallel methods.

Assuming that a hole-hole system is identical to a particle-particle system, one may utilize Pandya's theorem to obtain the states of ^{40}K in terms of the measured excitation energies of ^{46}K. As previously discussed, the simplest shell model picture of the lowest-lying levels of ^{46}K can be described by the configuration $\pi d_{3/2}^{-1}\nu f_{7/2}^{-1}$, i.e. a proton hole in the $d_{3/2}$ shell and a neutron hole in the $f_{7/2}$ shell.

Pandya's relation becomes:

$$E_J(^{40}K) = -\sum_{J_0}(2J_0+1)W(\tfrac{3}{2}\,\tfrac{7}{2}\,\tfrac{7}{2}\,\tfrac{3}{2},JJ_0)E_{J_0}(^{46}K) + C \qquad (26)$$

where $J_0 = 2,3,4,5$ are from jj coupling of the proton and neutron holes.

The results are shown in table V-2. It is clear that there is little, if any, correspondence between the separa-

Table V-1

Calculated energy levels of ^{38}Cl from ^{40}K using Pandya's theorem

J^{π}	$E^{*}_{calculated}$	$E^{*}_{experimental}$ † (MeV)
2^-	0.000	0.000
5^-	0.696	0.671
3^-	0.748	0.755
4^-	1.323	1.309

Table V-2

Calculated energy levels of ^{40}K from ^{46}K using Pandya's theorem

J^{π}	$E^{*}_{calculated}$	$E^{*}_{experimental}$ † (MeV)
4^-	0.138	0.000
3^-	0.192	0.030
2^-	0.000	0.800
5^-	0.728	0.892

† These values were obtained from ref. 33 All of these $E^{*}_{experimental}$ energies are known to an accuracy of 0.2 keV or better.

tion and order of the calculated and experimental ^{40}K states. The reasons for this will now be outlined.

V.2 $d_{3/2}$-$s_{1/2}$ spacing and configuration mixing effects

It has been observed experimentally[35,36] that the spacing between the $d_{3/2}$ and $s_{1/2}$ proton excitation states changes in a very interesting fashion. This separation steadily decreases with increasing atomic mass in the potassium isotopes and, eventually, the order of these states is reversed. This is illustrated in figure V-1 where the excitation energy of a $s_{1/2}$ hole in $^{A}_{19}K$, relative to the $d_{3/2}$ level, is plotted against the mass number A[33,37].

The cause for this trend is simply that the single particle energies have been altered by the increasing excess of neutrons in these potassium isotopes[38]. For each of these isotopes, there is a proton hole present which corresponds to the removal of a particle. As the $d_{3/2}f_{7/2}$ orbital overlap would be much greater than for a $s_{1/2}f_{7/2}$ overlap, one would expect a greater inter-nucleon interaction for the former configuration. Thus, it would become increasingly easier to remove a proton from the $s_{1/2}$ shell as neutrons are added, ultimately leading to the depression of the $s_{1/2}$ level with respect to the $d_{3/2}$ shell. Configuration mixing effects may also be responsible for the lowering of the $s_{1/2}$ level[38].

Figure V-1

Figure V-1

The energy of the $s_{1/2}$ hole in ${}^{A}_{19}K$, relative to the $d_{3/2}$ state, is plotted against the mass number A. The single hole energies (and J^{π} assignments) for these odd A isotopes are obtained from references 33 and 37.

50b

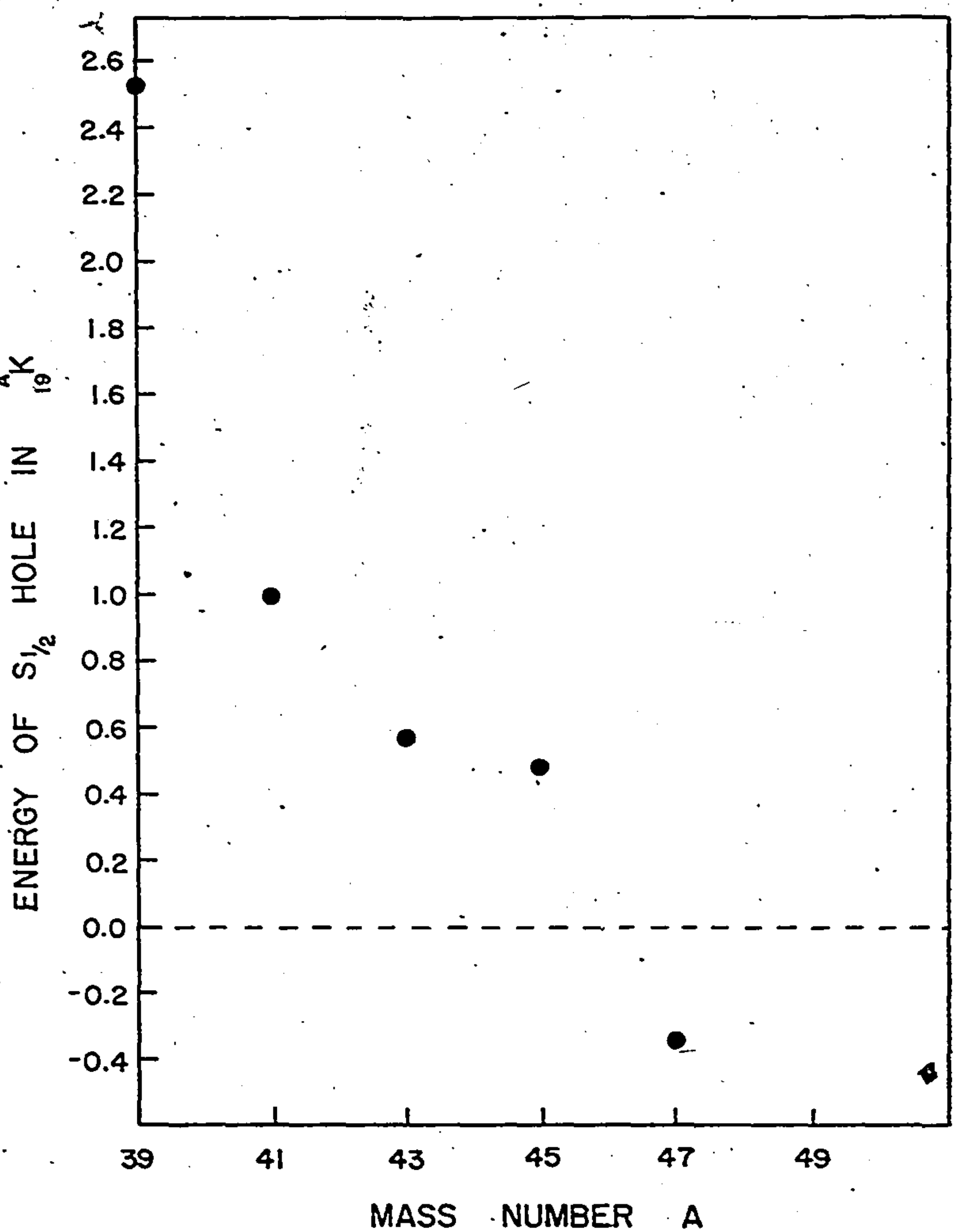

ENERGY OF $S_{1/2}$ HOLE IN $^{A}_{19}K$
2.6
2.4
2.2
2.0
1.8
1.6
1.4
1.2
1.0
0.8
0.6
0.4
0.2
0.0
-0.2
-0.4
39
41
43
45
47
49
MASS NUMBER A

The proximity of the $s_{1/2}$ and $d_{3/2}$ states in ^{46}K (refer to figure V-1) leads to complications in the form of configuration mixing. Neglecting configuration mixing for the moment, one would anticipate the following spins and parities for the lowest levels of ^{46}K:

Configuration	J^{π}
$\pi d_{3/2}^{-1} \nu f_{7/2}^{-1}$	$2^-, 3^-, 4^-, 5^-$
$\pi s_{1/2}^{-1} \nu f_{7/2}^{-1}$	$3^-, 4^-$

These spins and parities correspond to those seen by Daehnick et.al.[2] (and confirmed by our results) for the lowest six states. The configuration mixing would be expected to occur between the pair of 3^- states and, similarly, between the two 4^- states.

Because of the assumption made earlier about a hole-hole system being equivalent to a particle-particle system, it may be wise to now compare the low-lying levels of ^{46}K (hole-hole) to those of ^{38}Cl (particle-particle). Energy level diagrams of ^{46}K, ^{40}K, and ^{38}Cl are shown in figure V-2(a)[23,33]. Keeping in mind that the lowest ^{38}Cl states may be described as nearly pure $\pi d_{3/2} \nu f_{7/2}$ configurations, one observes that the 3^- and 4^- states are located at higher excitation energies than the 2^- and 5^- states in ^{38}Cl (as well as higher than the corresponding 3^- and 4^- levels in ^{46}K). The spacing of the 2^- and 5^- levels in ^{38}Cl appears to correspond rather well to the spacing of these nearly pure $(\pi d_{3/2}^{-1}\nu f_{7/2}^{-1})$ 2^- and 5^- levels in ^{46}K[31]. It appears from this comparison that one set of 3^- and 4^- levels has been depressed below and the remaining set has been raised above the location of the 3^- and 4^- states in the pure $\pi d_{3/2}\nu f_{7/2}$ configuration.

Following the discussion of Daehnick and Sherr[31], the effect of configuration mixing for states with small separations leads to the depression of one of the resultant levels with a spin and parity J^π. This lowering effect will tend to increase when a greater amount of configuration mixing occurs. The remaining states with the identical J^π undergo less drastic displacements from the zero-order energy. The observations noted in the previous paragraph tend to bear out these expectations. It is this shifting of the mixed levels that is the source of the discrepancies in table V-2. By examining equation (26), it can be seen that since a summation over each of the levels J_0 in ^{46}K is required (including the depressed 3^- and 4^- states) each of the values of E_J must necessarily be thrown out.

A schematic diagram of the lowest configurations of ^{46}K is presented in figure V-2(b). A neutron hole is shown in the $f_{7/2}$ shell and a rather hesitant proton hole is shown in the $s_{1/2}$-$d_{3/2}$ shell region. It should be pointed out that the single particle energy levels for neutrons differ some-

Figures V-2 a), b)

Figure V-2

a) The energy level diagrams for ^{46}K, ^{40}K, and ^{38}Cl obtained from references 23 and 33.

b) A simplified representation of the lowest configurations for ^{46}K as $\pi(d_{3/2}-s_{1/2})^{-1}\nu f_{7/2}^{-1}$.

536

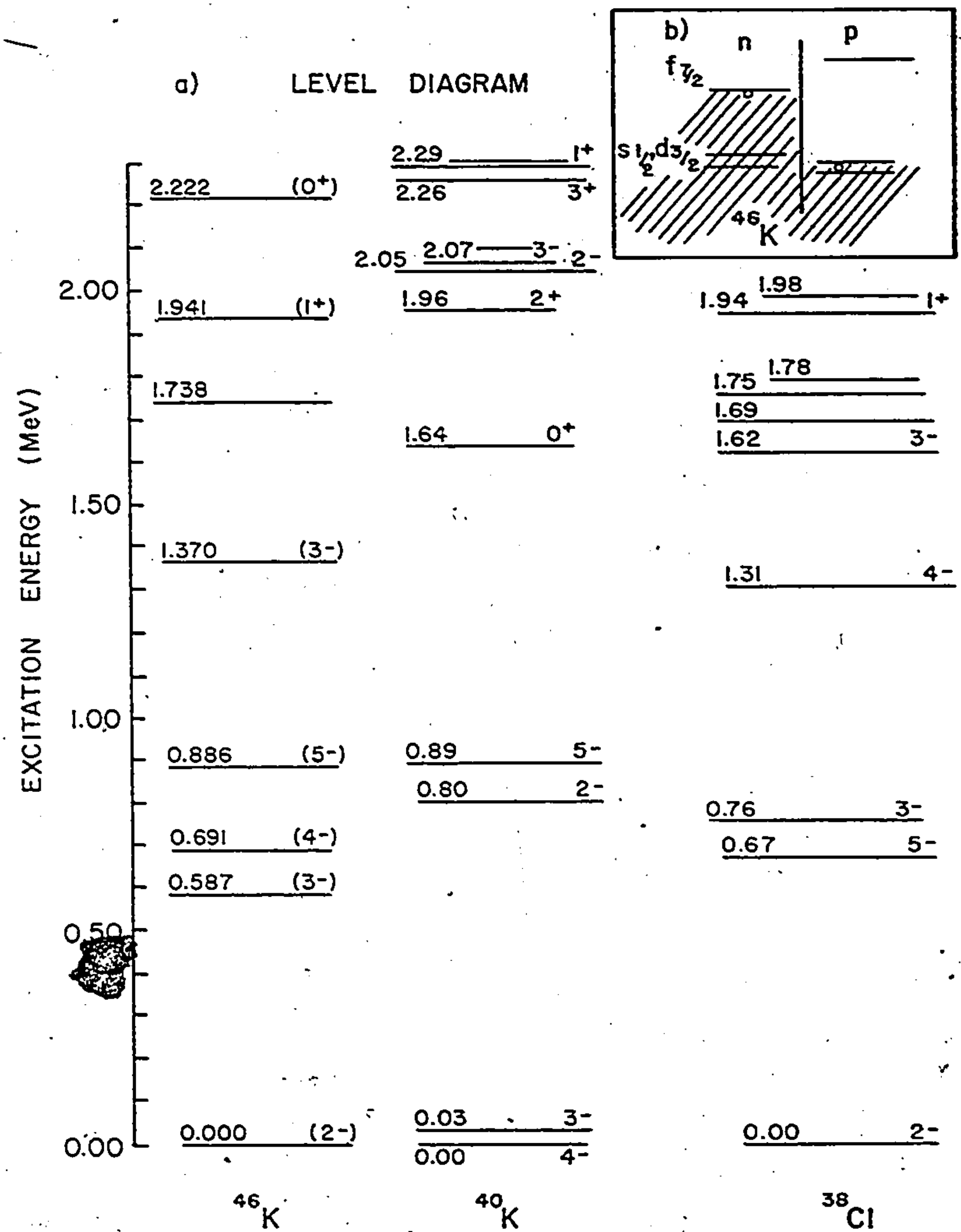

a) LEVEL DIAGRAM
EXCITATION ENERGY (MeV)
2.00
1.50
1.00
0.50
0.00
2.222 (0+)
1.941 (1+)
1.738
1.370 (3-)
0.886 (5-)
0.691 (4-)
0.587 (3-)
0.000 (2-)
2.29 1+
2.26 3+
2.05 2.07 3- 2-
1.96 2+
1.64 0+
0.89 5-
0.80 2-
0.03 3-
0.00 4-
1.94 1.98 1+
1.75 1.78
1.69
1.62 3-
1.31 4-
0.76 3-
0.67 5-
0.00 2-
46K
40K
38Cl
b) n p
f7/2
s1/2,d3/2
46K

what from those for the protons. The main reasons for this effect are the result of electrostatic repulsion and nuclear interaction effects between the excess neutrons and the proton hole[38].

If the arguments advanced in the last chapter for a $J^{\pi} = 1^{+}$ assignment to the 1.941 MeV state are accepted, then it becomes clear that this level does not belong to either of the negative parity multiplets discussed so far. Daehnick and Sherr[31] have used the single hole energies from ^{47}K and ^{47}Ca to predict a 2.6 MeV gap between the zero-order 1^{+} level and the centroid of the negative parity states. It has been proposed[31,39] that a mixture of $\pi d^{-1}_{3/2}\nu f^{8}_{7/2}d^{-1}_{3/2}$, $\pi s^{-1}_{1/2}\nu f^{8}_{7/2}d^{-1}_{3/2}$, and $\pi s^{-1}_{1/2}\nu f^{8}_{7/2}s^{-1}_{1/2}$ configurations may be responsible for the appreciable lowering of this state.

V.3 Consequences of mixing

Daehnick et.al.[2] have examined the consequences of configuration mixing for ^{46}K and the highlights from his discussion are presented below. The various calculations and plots to be mentioned may be found in this reference.

Intense coherence effects could account for the augmented cross-sections for such levels as the 4^{-} state at 0.691 MeV and the 1^{+} state at 1.941 MeV as well as for the weak cross-sections for the 3^{-} state at 0.587 MeV and the 4^{-} state at 1.738 MeV. As an outcome of configuration mixing, one of the resultant states J^{π} would demonstrate constructive coherence effects in the direct deuteron transfer amplitudes. In contrast, the other orthogonal J^{π} level would exhibit destructive coherent effects. Plots of DWBA predictions for the ratio of the cross-sections, for a given L, of constructive to destructive states against the sf-df mixing parameter α were obtained. By comparing these plots with existing data, experimental values of α were procured. This led to empirical wavefunctions which agreed rather well with theoretical wavefunctions obtained from Kuo G bare[40], Kuo plus core polarization[40], and Bertsch G bare calculations[41].

For the 17 MeV deuterons used by Daehnick, DWBA calculations indicated that L=3 deuteron transfer strongly dominated the observed cross-section over L=5 transfer. The wavefunctions obtained show that one should expect nearly total cancellation for the (d,α) and (p,^{3}He) L=3 transition amplitudes for the higher 4^- state at 1.738 MeV. This may also explain, in part, the rapid fluctuations in cross-section for this state with energy. The lower 4^- state (at 0.691 MeV) should, according to the wavefunctions, show constructive interference which partially explains the large cross-section. Similarly, the wavefunctions predict constructive coherence for the 3^- level at 1.370 MeV and destructive coherence for the 3^- state at 0.587 MeV (although the ratio for these two was not quite as impressive as in the 4^- case).

Although there was good agreement between the empirical and theoretical wavefunctions, the differences were sufficient to cause a wide variance in the calculated energy levels and matrix elements. Calculations performed with Kuo-Brown matrix elements incorporating core polarization corrections[40] yielded the most favourable results in terms of the spacing and order of the levels.

Preliminary calculations for positive parity states were also carried out. Unfortunately, the uncertainty in the neutron single particle energies for the $s_{1/2}$ and $d_{3/2}$ levels made the results somewhat inconclusive. In fact, the only useful outcome from this calculation was that a 1^+ level consistently appeared as the lowest of the positive parity states, as expected.

CHAPTER VI

CONCLUDING REMARKS

The tensor analyzing powers T_{20} from the $^{48}Ca(\vec{d},\alpha)^{46}K$ experiment indicate the following parities for the lowest lying states:

<u>unnatural parity</u>: ground state, 0.691, 1.738, and 1.941 MeV

<u>natural parity</u>: 0.587 and 0.886 MeV.

In addition, a tentative natural parity assignment was made to the 1.370 MeV level. These results have confirmed the most recent spin and parity assignments from Daehnick et.al.[2]. There does not appear to be any indication of other states below 2 MeV that can be populated by a (d,α) reaction.

The advantage of using this polarized deuteron technique lies in the fact that it is independent of the reaction mechanism and hence does not require the various assumptions made in the analysis of the other experiments. However, to obtain full spin-parity information, the other types of experiments must be performed.

Configuration mixing effects, arising from the closely spaced $d_{3/2}$-$s_{1/2}$ proton levels, appear to be very prominent in ^{46}K. Consequently, Pandya calculations of the order and spacing of the lowest states of ^{40}K did not at all correspond to the experimental excitation energies.

Two items remain incomplete: an investigation of higher levels and a more definite parity assignment for the 1.370 MeV state are required. The procedure involved may be difficult and extremely time consuming. In many cases, the beam energies used in other experiments are well beyond the capabilities of the McMaster tandem accelerator. As compound nuclear effects would probably be significant at these lower energies, a yield curve of the cross-section of a level as a function of the beam energy could be made. The $(\vec{d},\alpha)$ experiment could then be performed at the energies giving the maximum cross-sections in the particular level of interest.

Levels at 4.34 MeV and 5.95 MeV have been assigned J^{π}'s of (3^+) and (7^+) by Frascaria et.al.[39] using 80 MeV deuterons on ^{48}Ca. One could attempt to observe these levels at the lower beam energies available and thereby make a parity assignment.

Some or all of the following levels have been seen by Daehnick and Sherr[31] and Dupont[30]: 2.79 (2^+), 2.97 (4^-), 3.38, and 3.61 MeV using $(p,{}^3He)-(p,t)$ analog comparison experiments. The procedure outlined above could be attempted, but it may be met with very little success as none of these peaks have been distinguished from the background in any of the reported (d,α) spectra. As well, a $J^{\pi} = 0^{+}$ assignment has been made to levels at 2.22 and 11.47 MeV[30,31]. The latter state is believed to be a T=5 analog for the ground state of ^{44}Ar[30]. Unfortunately, if this assignment is correct, then there is little the $(\vec{d},\alpha)$ experiment can accomplish near 0° as a result of equation 13 in chapter II.

The 2.97 MeV level is of particular interest as it was believed to be from one of the negative parity multiplets although it was situated much higher in excitation energy than anticipated[31]. The 1.738 MeV level was later given a 4^{-} assignment by Daehnick et.al.[2]; our results only confirm that this is an unnatural parity state. A $(p,{}^{3}He)-(p,t)$ analog comparison experiment would probably be the most profitable way to obtain the angular distribution for this state (as well as for the other 2-4 MeV levels). One would, of course, require more complete results and an improved DWBA L curve fit than previously made before a definite J^{π} can be assigned to this level.

References

1. W. W. Daehnick, J. Orloff, T. Canada, and T. S. Bhatia, Bull. Am. Phys. Soc. 16, 555 (1971).

2. W. W. Daehnick, J. H. Orloff, T. Canada, and T. S. Bhatia, Phys. Rev. C 10, 136 (1974).

3. D. T. Petty, Ph.D. thesis, McMaster University, 1976.

4. A. Marinov and J. R. Erskine, Phys. Lett. 14, 46 (1965).

5. N. K. Glendenning, Ann. Rev. Nucl. Sci. 13, 191 (1963).

6. N. K. Glendenning, Phys. Rev. 137, B 102 (1965).

7. J. A. Kuehner, P. W. Green, G. D. Jones, and D. T. Petty, Phys. Rev. Lett. 35, 423 (1975).

8. D. T. Petty, J. A. Kuehner, J. Szücs, P. W. Green, and G. D. Jones, Phys. Rev. C 14, 12 (1976).

9. D. T. Petty, P. G. Ikossi, J. A. Kuehner, and J. Szücs, Phys. Rev. C 14, 908 (1976).

10. M. Jacob and G. C. Wick, Ann. Phys. 7, 404 (1959).

11. T. Ericson, Nucl. Phys. 17, 250 (1960).

12. T. Ericson, Phys. Lett. 4, 258 (1963).

13. D. O. Boerma, W. Grüebler, V. König, P. A. Schmelzbach, and R. Risler, Nucl. Phys. A255, 275 (1975).

14. A. A. Pilt, private communication.

15. J. W. McKay, M.Sc. thesis, McMaster University, 1976.

16. H. A. Enge, Nucl. Instr. Meth. 28, 125 (1964).

17. J. E. Spencer and H. A. Enge, Nucl. Instr. Meth. 49, 181 (1967).

18. J. L. C. Ford Jr., P. H. Stelson, and R. L. Robinson, Nucl. Instr. Meth. 98, 199 (1972).

19. H. W. Fulbright, R. G. Markham, and W. A. Lanford, Nucl. Instr. Meth. 108, 125 (1973).

20. D. H. Wilkinson. Ionization Chambers and Counters. Cambridge, Mass.: Cambridge University Press, 1950.

21. J. Sharpe. Nuclear Radiation Detectors. London: Methuen, 1955.

22. H. A. Enge, Rev. Sci. Instr. 29, 885 (1958).

23. R. L. Auble, et.al., Nuclear Data Sheets A=46, 199, 203, Vol. 24, No. 1, May 1978.

24. R. M. DelVecchio, Phys. Rev. C 3, 1989 (1971).

25. E. Rivet, R. H. Pehl, J. Cerny, and B. G. Harvey, Phys. Rev. 141, 1021 (1966).

26. C. C. Lu, M. S. Zisman, and B. G. Harvey, Phys. Rev. 186, 1086 (1969).

27. J. H. Orloff and W. W. Daehnick, Bull. Am. Phys. Soc. 15, 47 (1970).

28. M. Paul, A. Marinov, Ch. Drory, J. Burde, E. Navon, and Sh. Morderchai, Nucl. Phys. A168, 267 (1971).

29. Y. Dupont, P. Martin, and M. Chabre, Phys. Lett. 31B, 68 (1970).

30. Y. Dupont, P. Martin, and M. Chabre, Phys. Rev.C 7, 637 (1973).

31. W. W. Daehnick and R. Sherr, Phys. Rev. C 7, 150 (1973).

32. S. P. Pandya, Phys. Rev. 103, 956 (1956).

33. P. M. Endt and C. Van der Leun, A = 21-44, Nucl. Phys. A310, 1 (1978).

34. S. Goldstein and I. Talmi, Phys. Rev. 102, 589 (1956).

35. R. Santo, R. Stock, J. H. Bjerregaard, O. Hansen, O. Nathan, R. Chapman, and S. Hinds, Nucl. Phys. A118, 409 (1968).

36. J. H. Bjerregaard, O. Hansen, O. Nathan, R. Stock, R. Chapman, and S. Hinds, Phys. Lett. 24B, 568 (1967).

37. J. R. Beene, M. L. Halbert, et.al., Nuclear Data Sheets, A = 45, 47, 110, Vol. 22, No. 1, Sept. 1977.

38. G. Sartoris and L. Zamick, Phys. Rev. 167, 1035 (1968).

39. N. Frascaria, J. P. Didelez, J. P. Garron, E. Gerlic, and J. C. Roynette, Phys. Rev. C 10, 1422 (1974).

40. T. T. S. Kuo and G. E. Brown, Nucl. Phys. A114, 241 (1968).

41. G. F. Bertsch, The Practitioner's Shell Model. Amsterdam: North-Holland Publishing Company, 1972.

Miscellaneous References

A. de Shalit and I. Talmi. Nuclear Shell Theory. New York: Academic Press Inc., 1963.

P. J. Ellis, M. Strayer, and M. F. Werby, Phys. Rev. C 19, 536 (1979).

M. Rotenberg, R. Bivins, N. Metropolis, and J. K. Wooten Jr. The 3-j and 6-j Symbols. Cambridge, Mass: Technology Press, 1959.

R. R. Roy and B. P. Nigam. Nuclear Physics - Theory and Experiment. New York: John Wiley & Sons, Inc., 1967.

Nuclear Energy Level References

F. Ajzenberg-Selove and T. Lauritsen, A = 5-10, Nucl. Phys. A227, 1 (1974).

F. Ajzenberg-Selove, A = 11-12, Nucl. Phys. A248, 1 (1975).

F. Ajzenberg-Selove, A = 13-15, Nucl. Phys. A268, 1 (1976).

33 P. M. Endt and C. Van der Leun, A = 21-44, Nucl. Phys. A310, 1 (1978).

37 J. R. Beene, M. L. Halbert, et.al., Nuclear Data Sheets, A = 45, 47, 110, Vol. 22, No. 1, Sept. 1977.

23 R. L. Auble, et.al., Nuclear Data Sheets, A = 46, 199, 203, Vol. 24, No. 1, May 1978.